IEEE SA
STANDARDS ASSOCIATION

IEEE Guide for the Definition of Incident Power Density to Correlate Surface Temperature Elevation

STANDARDS

IEEE Standards Coordinating Committee 39

Developed by the
IEEE International Committee on Electromagnetic Safety

IEEE Std 2889™-2021

IEEE
AVA Documents
Document Sharing Hub
Authorized licensed use limited to: Tsinghua University. Downloaded on March 06,2026 at 22:42:56 UTC from IEEE Xplore. Restrictions apply.
Full document details: IEEE 2889-2021

IEEE Guide for the Definition of Incident Power Density to Correlate Surface Temperature Elevation

Developed by the

IEEE International Committee on Electromagnetic Safety

Approved 23 September 2021

IEEE SA Standards Board

Documents
Document Sharing Hub

Authorized licensed use limited to: Tsinghua University. Downloaded on March 06,2026 at 22:42:56 UTC from IEEE Xplore. Restrictions apply.

Full document details: IEEE 2889-2021

Abstract: Guidance on the definition of the incident power density in correlation with surface temperature elevation in the frequency range from 6 GHz to 300 GHz is provided. Using numerical simulations or measurement, this guide is also applicable to compliance assessment of wireless products operating in millimeter wave frequencies.

Keywords: dosimetry modeling, electromagnetic dosimetry, electromagnetic safety, IEEE 2889™, incident power density definition, millimeter wave exposure, numerical dosimetry, standardization, temperature rise, thermal dosimetry

The Institute of Electrical and Electronics Engineers, Inc.
3 Park Avenue, New York, NY 10016-5997, USA

Copyright © 2021 by The Institute of Electrical and Electronics Engineers, Inc.
All rights reserved. Published 17 December 2021. Printed in the United States of America.

IEEE is a registered trademark in the U.S. Patent & Trademark Office, owned by The Institute of Electrical and Electronics Engineers, Incorporated.

PDF: ISBN 978-1-5044-8015-4 STD24974
Print: ISBN 978-1-5044-8016-1 STDPD24974

IEEE prohibits discrimination, harassment, and bullying.
For more information, visit https://www.ieee.org/about/corporate/governance/p9-26.html.
No part of this publication may be reproduced in any form, in an electronic retrieval system or otherwise, without the prior written permission of the publisher.

Documents
Document Sharing Hub

Authorized licensed use limited to: Tsinghua University. Downloaded on March 06,2026 at 22:42:56 UTC from IEEE Xplore. Restrictions apply.

Full document details: IEEE 2889-2021

Important Notices and Disclaimers Concerning IEEE Standards Documents

IEEE Standards documents are made available for use subject to important notices and legal disclaimers. These notices and disclaimers, or a reference to this page (https://standards.ieee.org/ipr/disclaimers.html), appear in all standards and may be found under the heading "Important Notices and Disclaimers Concerning IEEE Standards Documents."

Notice and Disclaimer of Liability Concerning the Use of IEEE Standards Documents

IEEE Standards documents are developed within the IEEE Societies and the Standards Coordinating Committees of the IEEE Standards Association (IEEE SA) Standards Board. IEEE develops its standards through an accredited consensus development process, which brings together volunteers representing varied viewpoints and interests to achieve the final product. IEEE Standards are documents developed by volunteers with scientific, academic, and industry-based expertise in technical working groups. Volunteers are not necessarily members of IEEE or IEEE SA, and participate without compensation from IEEE. While IEEE administers the process and establishes rules to promote fairness in the consensus development process, IEEE does not independently evaluate, test, or verify the accuracy of any of the information or the soundness of any judgments contained in its standards.

IEEE does not warrant or represent the accuracy or completeness of the material contained in its standards, and expressly disclaims all warranties (express, implied and statutory) not included in this or any other document relating to the standard, including, but not limited to, the warranties of: merchantability; fitness for a particular purpose; non-infringement; and quality, accuracy, effectiveness, currency, or completeness of material. In addition, IEEE disclaims any and all conditions relating to results and workmanlike effort. In addition, IEEE does not warrant or represent that the use of the material contained in its standards is free from patent infringement. IEEE Standards documents are supplied "AS IS" and "WITH ALL FAULTS."

Use of an IEEE standard is wholly voluntary. The existence of an IEEE Standard does not imply that there are no other ways to produce, test, measure, purchase, market, or provide other goods and services related to the scope of the IEEE standard. Furthermore, the viewpoint expressed at the time a standard is approved and issued is subject to change brought about through developments in the state of the art and comments received from users of the standard.

In publishing and making its standards available, IEEE is not suggesting or rendering professional or other services for, or on behalf of, any person or entity, nor is IEEE undertaking to perform any duty owed by any other person or entity to another. Any person utilizing any IEEE Standards document, should rely upon his or her own independent judgment in the exercise of reasonable care in any given circumstances or, as appropriate, seek the advice of a competent professional in determining the appropriateness of a given IEEE standard.

IN NO EVENT SHALL IEEE BE LIABLE FOR ANY DIRECT, INDIRECT, INCIDENTAL, SPECIAL, EXEMPLARY, OR CONSEQUENTIAL DAMAGES (INCLUDING, BUT NOT LIMITED TO: THE NEED TO PROCURE SUBSTITUTE GOODS OR SERVICES; LOSS OF USE, DATA, OR PROFITS; OR BUSINESS INTERRUPTION) HOWEVER CAUSED AND ON ANY THEORY OF LIABILITY, WHETHER IN CONTRACT, STRICT LIABILITY, OR TORT (INCLUDING NEGLIGENCE OR OTHERWISE) ARISING IN ANY WAY OUT OF THE PUBLICATION, USE OF, OR RELIANCE UPON ANY STANDARD, EVEN IF ADVISED OF THE POSSIBILITY OF SUCH DAMAGE AND REGARDLESS OF WHETHER SUCH DAMAGE WAS FORESEEABLE.

Documents
Document Sharing Hub

Authorized licensed use limited to: Tsinghua University. Downloaded on March 06,2026 at 22:42:56 UTC from IEEE Xplore. Restrictions apply.

Full document details: IEEE 2889-2021

Translations

The IEEE consensus development process involves the review of documents in English only. In the event that an IEEE standard is translated, only the English version published by IEEE is the approved IEEE standard.

Official statements

A statement, written or oral, that is not processed in accordance with the IEEE SA Standards Board Operations Manual shall not be considered or inferred to be the official position of IEEE or any of its committees and shall not be considered to be, nor be relied upon as, a formal position of IEEE. At lectures, symposia, seminars, or educational courses, an individual presenting information on IEEE standards shall make it clear that the presenter's views should be considered the personal views of that individual rather than the formal position of IEEE, IEEE SA, the Standards Committee, or the Working Group.

Comments on standards

Comments for revision of IEEE Standards documents are welcome from any interested party, regardless of membership affiliation with IEEE or IEEE SA. However, **IEEE does not provide interpretations, consulting information, or advice pertaining to IEEE Standards documents**.

Suggestions for changes in documents should be in the form of a proposed change of text, together with appropriate supporting comments. Since IEEE standards represent a consensus of concerned interests, it is important that any responses to comments and questions also receive the concurrence of a balance of interests. For this reason, IEEE and the members of its Societies and Standards Coordinating Committees are not able to provide an instant response to comments, or questions except in those cases where the matter has previously been addressed. For the same reason, IEEE does not respond to interpretation requests. Any person who would like to participate in evaluating comments or in revisions to an IEEE standard is welcome to join the relevant IEEE working group. You can indicate interest in a working group using the Interests tab in the Manage Profile & Interests area of the IEEE SA myProject system. An IEEE Account is needed to access the application.

Comments on standards should be submitted using the Contact Us form.

Laws and regulations

Users of IEEE Standards documents should consult all applicable laws and regulations. Compliance with the provisions of any IEEE Standards document does not constitute compliance to any applicable regulatory requirements. Implementers of the standard are responsible for observing or referring to the applicable regulatory requirements. IEEE does not, by the publication of its standards, intend to urge action that is not in compliance with applicable laws, and these documents may not be construed as doing so.

Data privacy

Users of IEEE Standards documents should evaluate the standards for considerations of data privacy and data ownership in the context of assessing and using the standards in compliance with applicable laws and regulations.

Copyrights

IEEE draft and approved standards are copyrighted by IEEE under US and international copyright laws. They are made available by IEEE and are adopted for a wide variety of both public and private uses. These

Documents
Document Sharing Hub

Authorized licensed use limited to: Tsinghua University. Downloaded on March 06,2026 at 22:42:56 UTC from IEEE Xplore. Restrictions apply.

Full document details: IEEE 2889-2021

include both use, by reference, in laws and regulations, and use in private self-regulation, standardization, and the promotion of engineering practices and methods. By making these documents available for use and adoption by public authorities and private users, IEEE does not waive any rights in copyright to the documents.

Photocopies

Subject to payment of the appropriate licensing fees, IEEE will grant users a limited, non-exclusive license to photocopy portions of any individual standard for company or organizational internal use or individual, non-commercial use only. To arrange for payment of licensing fees, please contact Copyright Clearance Center, Customer Service, 222 Rosewood Drive, Danvers, MA 01923 USA; +1 978 750 8400; https://www.copyright.com/. Permission to photocopy portions of any individual standard for educational classroom use can also be obtained through the Copyright Clearance Center.

Updating of IEEE Standards documents

Users of IEEE Standards documents should be aware that these documents may be superseded at any time by the issuance of new editions or may be amended from time to time through the issuance of amendments, corrigenda, or errata. An official IEEE document at any point in time consists of the current edition of the document together with any amendments, corrigenda, or errata then in effect.

Every IEEE standard is subjected to review at least every 10 years. When a document is more than 10 years old and has not undergone a revision process, it is reasonable to conclude that its contents, although still of some value, do not wholly reflect the present state of the art. Users are cautioned to check to determine that they have the latest edition of any IEEE standard.

In order to determine whether a given document is the current edition and whether it has been amended through the issuance of amendments, corrigenda, or errata, visit IEEE Xplore or contact IEEE. For more information about the IEEE SA or IEEE's standards development process, visit the IEEE SA Website.

Errata

Errata, if any, for all IEEE standards can be accessed on the IEEE SA Website. Search for standard number and year of approval to access the web page of the published standard. Errata links are located under the Additional Resources Details section. Errata are also available in IEEE Xplore. Users are encouraged to periodically check for errata.

Patents

IEEE Standards are developed in compliance with the IEEE SA Patent Policy.

IMPORTANT NOTICE

IEEE Standards do not guarantee or ensure safety, security, health, or environmental protection, or ensure against interference with or from other devices or networks. IEEE Standards development activities consider research and information presented to the standards development group in developing any safety recommendations. Other information about safety practices, changes in technology or technology implementation, or impact by peripheral systems also may be pertinent to safety considerations during implementation of the standard. Implementers and users of IEEE Standards documents are responsible for determining and complying with all appropriate safety, security, environmental, health, and interference protection practices and all applicable laws and regulations.

Documents
Document Sharing Hub

Authorized licensed use limited to: Tsinghua University. Downloaded on March 06,2026 at 22:42:56 UTC from IEEE Xplore. Restrictions apply.

Full document details: IEEE 2889-2021

Participants

At the time this IEEE guide was completed, the Working Group 5 of Subcommittee 6 had the following membership:

Walid El Hajj, *Chair*

Quirino Balzano
Giorgi Bit-Babik
J. C. Chen
Andreas Christ
Valerio De Santis
Yinliang Diao
Martin Dockzat
Mark Douglas
Kevin Graf
Tim Harrington
Akimasa Hirata
Jafar Keshvari
Niels Kuster
Ilkka Laasko
Kun Li
Kai Niskala
Teruo Onishi
Yi Pan
Dragan Poljak
Alexander Prokop
John Roman
Greguy Saint-Pierre
Kensuke Sasaki
Glembo Tyler
Yao Zhen

The following members of the individual Standards Association balloting group voted on this guide. Balloters may have voted for approval, disapproval, or abstention.

Gilles Bargone
Matthew Butcher
C. Chou
Mark Douglas
Kenneth Foster
Kevin Graf
Werner Hoelzl
Kenneth Joyner
Wolfgang Kainz
Efthymios Karabetsos
Nam Kim
Yeou Song Lee
Yung-chiang Lee
Ting Li
David Maxson
Teruo Onishi
John Osepchuk
Alexander Prokop
Gary Smullin
Richard Tell
Karl Weber
Marvin Ziskin
Peter Zollman

When the IEEE SA Standards Board approved this guide on 23 September 2021, it had the following membership:

Gary Hoffman, *Chair*
Jon Walter Rosdahl, *Vice Chair*
John D. Kulick, *Past Chair*
Konstantinos Karachalios, *Secretary*

Edward A. Addy
Doug Edwards
Ramy Ahmed Fathy
J. Travis Griffith
Thomas Koshy
Joseph L. Koepfinger*
David J. Law
Howard Li
Daozhuang Lin
Kevin Lu
Daleep C. Mohla
Chenhui Niu
Damir Novosel
Annette Reilly
Dorothy Stanley
Mehmet Ulema
Lei Wang
F. Keith Waters
Karl Weber
Sha Wei
Howard Wolfman
Daidi Zhong

*Member Emeritus

Copyright © 2021 IEEE. All rights reserved.
Documents
Document Sharing Hub
Authorized licensed use limited to: Tsinghua University. Downloaded on March 06,2026 at 22:42:56 UTC from IEEE Xplore. Restrictions apply.
Full document details: IEEE 2889-2021

Introduction

This introduction is not part of IEEE Std 2889™-2021, IEEE Guide for the Definition of Incident Power Density to Correlate Surface Temperature Elevation.

In 1960, the American Standards Association approved the initiation of the Radiation Hazards Standards project under the co-development of the Department of the Navy and the Institute of Electrical and Electronics Engineers, Incorporated (IEEE; called the "Institute of Radio Engineers [IRE]" at the time). Prior to 1988, C95 standards were developed by Accredited Standards Committee C95 and submitted to the American National Standards Institute (ANSI) for approval and issuance as ANSI C95 standards. Between 1988 and 1990, the committee was converted to the "Standards Coordinating Committee 28 (SCC28)" under the development of the IEEE Standards Board. In 2001, the IEEE Standards Association Standards Board approved the name IEEE International Committee on Electromagnetic Safety (ICES) for SCC28 to better reflect the scope of the committee and its international membership. In accordance with the policies of the IEEE, C95 standards are issued and developed as IEEE standards and submitted to ANSI for recognition.

In June 1995, the IEEE Standards Board approved the establishment of "Standards Coordinating Committee 34 (SCC34), Product Performance Standards Relative to the Safe Use of Electromagnetic Energy." Standards developed by SCC34 do not specify limits for human exposure to electromagnetic fields, but refer to established limits found in science-based standards, such as IEEE Std C95.1™-2005, IEEE Standard for Safety Levels with Respect to Human Exposure to Radio Frequency Electromagnetic Fields, 3 kHz to 300 GHz.

In 2005, SCC28 and SCC34 became "Technical Committee 95" and "Technical Committee 34," respectively, under a new IEEE Standards Coordinating Committee, SCC39, which is now called "ICES."[1]

The present scope of IEEE ICES Technical Committee 95 (TC95) is as follows:

"Development of standards for the safe use of electromagnetic energy in the range of 0 Hz to 300 GHz relative to the potential hazards of exposure of man, volatile materials, and explosive devices to such energy. It is not intended to include infrared, visible, ultraviolet, or ionizing radiation. The committee will coordinate with other committees whose scopes are contiguous with ICES."

There are six TC95 subcommittees, each of whose area of responsibility is described as follows in correspondence with its designated subcommittee number:

- SC 1: Techniques, Procedures, Instrumentation, and Computation
- SC 2: Terminology, Units of Measurements, and Hazard Communication
- SC 3: Safety Levels with Respect to Human Exposure, 0 Hz to 3 kHz
- SC 4: Safety Levels with Respect to Human Exposure, 3 kHz to 300 GHz
- SC 5: Safety Levels with Respect to Electro-Explosive Devices
- SC 6: EMF Modeling and Dosimetry

This standard was prepared by WG5 of Subcommittee 6 of TC95.

[1] Standards Coordinating Committees are established by the IEEE SA Standards Board and provide a mechanism to oversee the development of standards that are beyond the scopes of individual technical committees within IEEE's societies.

Copyright © 2021 IEEE. All rights reserved.
Documents
Document Sharing Hub
Authorized licensed use limited to: Tsinghua University. Downloaded on March 06,2026 at 22:42:56 UTC from IEEE Xplore. Restrictions apply.
Full document details: IEEE 2889-2021

Contents

1. Overview 10
1.1 Introduction and objectives 10
1.2 Scope 11
1.3 Purpose 11
1.4 Word usage 12

2. Normative references 12

3. Definitions, acronyms, and abbreviations 12
3.1 General 12
3.2 Definitions 12
3.3 Acronyms and abbreviations 15

4. Physical and mathematical review of Poynting vector and power density 17
4.1 General 17
4.2 Poynting theorem 17
4.3 Poynting vector and power density 18
4.4 Comparison of the definitions of sPD 20

5. Assessment methodology 20
5.1 General 20
5.2 Numerical methods 20
5.3 Experimental methods 22
5.4 Evaluation and analysis of the results 24

6. Exposure configurations 26
6.1 General 26
6.2 Numerical antenna models 28
6.3 Numerical body models 31
6.4 Tissue parameters 36
6.5 Influence of incidence angles 39

7. Numerical results 39
7.1 General 39
7.2 Pooled temperature increase versus incident power density 40
7.3 Heating factors—statistical analysis 44
7.4 Pearson's correlation coefficients 48
7.5 Statistical significance test results 48
7.6 Summary 50
7.7 Impact of incidence angle 50

8. Experimental results 53
8.1 General 53
8.2 Free space measurements 53
8.3 Thermographic measurements 55

9. Comparison of simulations and measurements 56
9.1 General 56
9.2 Evaluation results 56
9.3 Summary and discussion 63

10. Discussion and conclusions 64
10.1 Correlation coefficients 64

Copyright © 2021 IEEE. All rights reserved.

Documents
Document Sharing Hub

Authorized licensed use limited to: Tsinghua University. Downloaded on March 06,2026 at 22:42:56 UTC from IEEE Xplore. Restrictions apply.

Full document details: IEEE 2889-2021

10.2 Heating factor 64
10.3 Incidence angle 64
10.4 General conclusions 64

Annex A (informative) Individual numerical results from participating laboratories 66
A.1 Dipole source 66
A.2 Dipole array 91
A.3 Cavity-fed dipole array 106
A.4 Patch antenna 108
A.5 Patch array 110
A.6 Pyramidal horn slotted array 114

Annex B (informative) Experimental results 119
B.1 Free space measurements 119

Annex C (informative) Bibliography 149

Copyright © 2021 IEEE. All rights reserved.
Documents
Document Sharing Hub
Authorized licensed use limited to: Tsinghua University. Downloaded on March 06,2026 at 22:42:56 UTC from IEEE Xplore. Restrictions apply.
Full document details: IEEE 2889-2021

IEEE Guide for the Definition of Incident Power Density to Correlate Surface Temperature Elevation

1. Overview

1.1 Introduction and objectives

International standards/guidelines (IEEE Std C95.1™-2019 [B13][2]; ICNIRP [B14]) for human exposure to electromagnetic fields have been recently updated and introduced new exposure limits in terms of dosimetric reference limits (DRL or basic restrictions) and exposure reference levels (ERLs). ERLs are practical and enable more efficient exposure compliance assessment compared to the evaluation of the dosimetric quantities against the DRLs. Exposure below the ERLs implicitly assumes that the DRLs are not violated in the exposed subjects.

In the frequency range 6 GHz to 300 GHz, the ERL is based on incident power density (IPD) and is defined for whole-body as well as local exposure conditions, with the latter applicable to devices operating in close proximity to the head and body. The DRLs are based on the epithelial power density (IEEE Std C95.1-2019 [B13]) or the absorbed power density (ICNIRP [B14]) averaged over a square shaped area of 1 cm^2 or 4 cm^2. Both quantities are measures for the power that is absorbed in the body. The DRLs are based on the quantification of the induced temperature increase at the body surface and are correlated with the ERLs via the plane wave reflection coefficient of the skin.

Because the plane wave reflection coefficient describes the correlation of incident and absorbed electromagnetic fields or radio frequency power only under far-field conditions, additional considerations are required for the near field. In the far field, the Poynting vector, which is used to calculate the averaged incident power density, is purely real, and the direction of its vector components—or the direction of the power flux—does not change over a period of the signal. In the near field of an antenna, this is no longer the case. Reactive fields may contribute to the absorption of electromagnetic energy in the exposed body (Kuster and Balzano [B17]), additional components of the Poynting vector may need to be considered for the definition of the incident power density, and the correlation of incident and epithelial power density using the plane wave transmission coefficient may not be sufficiently accurate. Several recent publications have shown that the traditional definition of the far-field zone is overly conservative, and that near-field effects can generally be neglected for distances larger than approximately $\lambda/2\pi$ from the antenna (Carrasco et al. [B1]; Christ et al. [B2]; Colombi et al. [B3]).

[2] The numbers in brackets correspond to those of the bibliography in Annex C.

Copyright © 2021 IEEE. All rights reserved.
Documents
Document Sharing Hub
Authorized licensed use limited to: Tsinghua University. Downloaded on March 06,2026 at 22:42:56 UTC from IEEE Xplore. Restrictions apply.
Full document details: IEEE 2889-2021

With the progress in development of the product compliance assessment standards, the importance of more precise and unambiguous IPD definition became apparent to facilitate practical evaluation procedures. One aspect of this definition is related to the IPD quantity averaged over the prescribed surface area where two different methods could be used:

— Only the components of IPD vectors normal to the averaging surface are used for averaging.

— The magnitude (norm) of IPD vectors are averaged over the area irrespective to the orientation.

As mentioned in the preceding paragraphs, in some near-field conditions (especially with oblique incident waves), these two definitions lead to different results. Since the high-frequency radio frequency (RF) exposure standard and guidelines are based on avoiding excessive heat induced in tissue, both expressions for the IPD are analyzed with respect to their correlation with tissue surface temperature rise. The temperature rise is evaluated for different stratified and anatomical body models exposed to antennas operating between 10 GHz and 90 GHz at distances from 2 mm to 150 mm. The evaluations are carried out numerically by different laboratories and several selected configurations are validated experimentally. The overall objective of the work presented here is to identify the definition of the IPD that yields the best correlation with the induced temperature increase.

Working Group 5 (WG5) within the IEEE/ICES TC95/SC6 was created with the objective to perform such study using computer simulations and measurements and—with the supporting data, analysis, and conclusions—contribute to the development of the compliance assessment standards for wireless products.

This guide provides a comparison between the two definitions of IPD in correlation with temperature rise. It describes the data generated by WG5 in this study and provides corresponding analysis and conclusions.

1.2 Scope

This document provides guidance on the definition of the incident power density in correlation with surface temperature elevation in the frequency range from 6 GHz to 300 GHz. Using numerical simulations or measurement, this guide is also applicable to compliance assessment of wireless products operating in millimeter wave frequencies.

1.3 Purpose

The incident power density (IPD) is generally spatially averaged over an averaging area. Two quantities may be used to define the spatially averaged IPD, either using the normal component of IPD vectors crossing the surface, or magnitude of IPD vectors (norm) averaged over an area independent of the orientation.

This document provides guidance for determining the appropriate definition of IPD. The guide examines theoretical, computational, and measurement data that are relevant to the validity of each method, taking into account the dependence of the IPD metric and its averaging methods on surface temperature rise in the frequency range 6 GHz to 300 GHz.

This guide might be used in the development of standards for the EMF exposure limits or in the EMF compliance assessment standards.

Copyright © 2021 IEEE. All rights reserved.
Documents
Document Sharing Hub
Authorized licensed use limited to: Tsinghua University. Downloaded on March 06,2026 at 22:42:56 UTC from IEEE Xplore. Restrictions apply.
Full document details: IEEE 2889-2021

1.4 Word usage

The word *shall* indicates mandatory requirements strictly to be followed in order to conform to the standard and from which no deviation is permitted (*shall* equals is *required to*).[3, 4]

The word *should* indicates that among several possibilities one is recommended as particularly suitable, without mentioning or excluding others; or that a certain course of action is preferred but not necessarily required (*should* equals is *recommended that*).

The word *may* is used to indicate a course of action permissible within the limits of the standard (*may* equals is *permitted to*).

The word *can* is used for statements of possibility and capability, whether material, physical, or causal (*can* equals is *able to*).

2. Normative references

This standard has no normative references.

3. Definitions, acronyms, and abbreviations

3.1 General

For the purposes of this document, the following terms and definitions apply. The following references should be consulted for terms not defined in this clause.

- *IEEE Standards Dictionary Online*[5]
- IEC Electropedia[6]
- ISO Online browsing platform[7]

3.2 Definitions

antenna: That part of a radio transmitting or receiving system which is designed to provide the required coupling between a transmitter or a receiver and the medium in which the radio wave propagates.

NOTE 1—In practice, the terminals of the antenna or the points to be considered as the interface between the antenna and the transmitter or receiver should be specified.[8]

NOTE 2—If a transmitter or receiver is connected to its antenna by a feed line, the antenna may be considered to be a transducer between the guided waves of the feed line and the radiated waves in space.

antenna sub-array: Subset of radiating elements in an array that are processed collectively.

NOTE—Two or more sub-arrays may share antenna elements.

[3] The use of the word *must* is deprecated and cannot be used when stating mandatory requirements, *must* is used only to describe unavoidable situations.
[4] The use of *will* is deprecated and cannot be used when stating mandatory requirements, *will* is only used in statements of fact.
[5] *IEEE Standards Dictionary Online* is available at: http://dictionary.ieee.org. An IEEE Account is required for access to the dictionary, and one can be created at no charge on the dictionary sign-in page.
[6] Available at http://www.electropedia.org/.
[7] Available at http://www.iso.org/obp.
[8] Notes in text, tables, and figures of a standard are given for information only and do not contain requirements needed to implement this standard.

Copyright © 2021 IEEE. All rights reserved.
Documents
Document Sharing Hub
Authorized licensed use limited to: Tsinghua University. Downloaded on March 06,2026 at 22:42:56 UTC from IEEE Xplore. Restrictions apply.
Full document details: IEEE 2889-2021

antenna array: Antenna composed of a number of radiating elements the inputs (or outputs) of which are processed collectively.

averaging area: Area A_{av} on the evaluation surface over which the spatial-average power density is calculated.

NOTE—The surface may be a square area with side length $L = \sqrt{A_{av}}$ or the cross-section of a sphere with radius $r = \sqrt{A_{av}/\pi}$.

combined uncertainty: Estimated standard deviation of the result obtained by combining the individual standard uncertainties of both Type A and Type B evaluations using the usual "root-sum-squares" method of combining standard deviations which were obtained by taking the positive square root of the estimated variances.

complex Poynting vector: Energy transfer per unit area for time harmonic signals, expressed in W/m^2:

$$\mathbf{P} = \mathbf{E} \times \mathbf{H}^*$$

where

E is the complex electric field vector amplitude

H is the magnetic field vector amplitude

* denotes the complex conjugate

dipole: Symmetrical antenna composed of conductors (usually rectilinear) and energized by a balanced feed.

expanded uncertainty: Quantity defining an interval about the result that is expected to encompass a distribution of values within a defined confidence interval that could reasonably be attributed to the measurand.

far field: Region of the field of an antenna where the ratio of the magnitude of the electric field (E-field) vector to the magnitude of the magnetic field (H-field) vector is equivalent to 377 Ω ± 10% within a minimum volume of $(\lambda/10)^3$.

heating factor: Factor defined as the ratio of steady state temperature in the skin to the incident power density.

half-wave dipole: A rectilinear dipole antenna whose total electrical length is about one half-wavelength.

instantaneous Poynting vector (P): Energy transfer per unit area per unit time, expressed in W/m^2:

$$P(t) = \mathcal{E}(t) \times \mathcal{H}(t)$$

where

$\mathcal{E}$ is the electric field vector, as a function of time

$\mathcal{H}$ is the magnetic field vector, as a function of time

local power density (PD): Local electromagnetic energy flux as a function of the Poynting vector.

NOTE 1—In this document, the PD is also referred to as *local power density* to distinguish it from the spatial-average power density.

Copyright © 2021 IEEE. All rights reserved.
Documents
Document Sharing Hub
Authorized licensed use limited to: Tsinghua University. Downloaded on March 06,2026 at 22:42:56 UTC from IEEE Xplore. Restrictions apply.
Full document details: IEEE 2889-2021

NOTE 2—The calculation of the PD as a function of the Poynting vector may be specified by local regulators.

NOTE 3—Some documents and national regulations consider the associated term *plane-wave equivalent power density,* which for uniform compliance evaluation purposes is applied regardless of whether the evaluation surface is in the far-field region. The *plane-wave equivalent power density* is defined as the square of the modulus of the local electric field (E-field) vector divided by two times the free space wave impedance. Its applicability in the close near field may require particular consideration if, e.g., the magnetic field is dominant for the absorption in the body.

near field: Region in which the far-field condition is not met.

peak spatial-average power density (psPD): Global maximum value of all *sPD* values defined on the evaluation surface:

$$psPD = \max_{r} \left\{ sPD(\mathbf{r}) \right\}$$

where

$\mathbf{r}$ is a point on the evaluation surface

NOTE—Multiple local maxima (secondary peak spatial-average power density values) may occur.

spatial-average power density (sPD): PD averaged over the averaging area A_{av} on the evaluation surface:

$$sPD(\mathbf{r}_0) = \frac{1}{A_{\text{av}}} \iint_{A_{\text{av}}} PD(\mathbf{r})\, dA$$

where

PD is the local power density

$\mathbf{r}_0$ is the point where sPD is evaluated

$\mathbf{r}$ is a point on the local averaging area

standard uncertainty: Estimated standard deviation of a result, equal to the positive square root of the estimated variance.

time averaged Poynting vector: Energy transfer per unit area for time harmonic signals averaged over one period of the signal frequency, expressed in W/m^2:

$$\boldsymbol{P}_{t\text{Av}} = \frac{1}{2} \Re \left\{ \boldsymbol{E} \times \boldsymbol{H}^* \right\}$$

where

$\boldsymbol{E}$ is the complex electric field vector amplitude

$\boldsymbol{H}$ is the complex magnetic field vector amplitude

* denotes the complex conjugate

uncertainty: Parameter, associated with the result of a measurement or simulation, that characterizes the dispersion of the values that could reasonably be attributed to the measurand.

NOTE 1—This term is used in the "uncertainty" approach.

NOTE 2—The parameter can be, for example, a standard deviation (or a given multiple of it), or a half-width of an interval having a stated level of confidence. Various ways of obtaining uncertainty are defined in the Guide to the Expression of Uncertainty in Measurement (GUM) (JCGM 100:2008 [B15]).

Copyright © 2021 IEEE. All rights reserved.
Documents
Document Sharing Hub
Authorized licensed use limited to: Tsinghua University. Downloaded on March 06,2026 at 22:42:56 UTC from IEEE Xplore. Restrictions apply.
Full document details: IEEE 2889-2021

NOTE 3—Uncertainty of measurement comprises, in general, many components. Some of these components can be evaluated from the statistical distribution of the results of a series of measurements and can be characterized by experimental standard deviations. The other components, which can also be characterized by standard deviations, are evaluated from the assumed probability distributions based on experience or other information.

uncertainty evaluation: Evaluation of uncertainty by the statistical analysis of series of observations (Type A) or by other means (Type B).

3.3 Acronyms and abbreviations

Symbol	Quantity	Unit	Dimensions
α	Attenuation coefficient	Reciprocal meter	1/m
P	Average (temporal) absorbed power	Watt	W
J	Current density	Ampere per square meter	A/m^2
σ	Electrical conductivity	Siemens per meter	S/m
E	Electric field strength	Volt per meter	V/m
W_c	Energy possessed by particles	Joule	J
f	Frequency	Hertz	Hz
h	Heat transfer coefficient	Watt per square meter per kelvin	$W/(m^2\ K)$
H	Magnetic field strength	Ampere per meter	A/m
ρ	Mass density	Kilogram per cubic meter	kg/m^3
A	Metabolic rate	Watt per cubic meter	W/m^3
B	Term associated with blood flow	Watt per cubic meter per kelvin	$W/(m^3\ K)$
$p\Delta T$	Peak temperature increase	Kelvin	K
δ	Penetration depth	Meter	m
μ	Permeability	Henry per meter	H/m
ε	Permittivity	Farad per meter	F/m
PD	Power density	Watt per square meter	W/m^2
sPD	Spatial-average power density	Watt per square meter	W/m^2
sPD_n	Spatial-average power density using normal component of Poynting vector; see Equation (5)	Watt per square meter	W/m^2
sPD_{tot}	Spatial-average power density using the norm of Poynting vector; see Equation (7)	Watt per square meter	W/m^2
pPD	Peak power density	Watt per square meter	W/m^2
$psPD$	Peak spatial-average power density	Watt per square meter	W/m^2
$psPD_n$	Peak spatial-average power density using normal component of Poynting vector; see Equation (5)	Watt per square meter	W/m^2
$psPD_{tot}$	Peak spatial-average power density using the norm of Poynting vector; see Equation (7)	Watt per square meter	W/m^2
SAR	Specific absorption rate	Watt per kilogram	W/kg
c	Specific heat capacity	Joule per kilogram per kelvin	J/(kg K)
T	Temperature	Kelvin	K
ΔT	Temperature increase	Kelvin	K
κ	Thermal conductivity	Watt per meter per kelvin	W/(m K)
λ	Wavelength	Meter	m
c	Speed of light in vacuum	Meter per second	m/s
η_0	Intrinsic impedance of free space	Ohms	Ω

Copyright © 2021 IEEE. All rights reserved.
Documents
Document Sharing Hub
Authorized licensed use limited to: Tsinghua University. Downloaded on March 06,2026 at 22:42:56 UTC from IEEE Xplore. Restrictions apply.
Full document details: IEEE 2889-2021

3.3.1 Physical quantities

NOTE—In this standard, temperature is quantified in degrees Celsius, as defined by: T (°C) = T (K) – 273.15.

3.3.2 Constants

Symbol	Physical constant	Magnitude
ε_0	Permittivity of free space	8.854×10^{-12} F/m
μ_0	Permeability of free space	$4\pi \times 10^{-7}$ H/m
c	Speed of light in vacuum	2.998×10^{8} m/s
η_0	Intrinsic impedance of free space	$\approx 377\ \Omega$[9]

3.3.3 Abbreviations

AUT	antenna under test
BC	boundary condition
BEM	boundary element method
CAD	computer-aided design
CL	confidence level
CPML	convolutional perfectly matched layer
DUT	device under test
E-field	electric field
EM	electromagnetic
FDTD	finite-difference time-domain
FEM	finite element method
FIT	finite integration technique
H-field	magnetic field
HF	heating factor
IPD	incident power density
OTA	over-the-air
PBHE	Pennes's bio-heat equation
PEC	perfect electric conductor
PML	perfectly matched layer
PD	power density
RF	radio frequency
RMS	root mean square

[9] According to the National Institute of Standards and Technology (NIST) (USA), the intrinsic impedance of a plane wave in a vacuum (η_0) is 376.730313461 Ω. This exact value of η_0 (derived as the square root of the ratio of vacuum permeability [μ_0] to vacuum permittivity [ε_0]) is approximately 377 Ω when rounded to the nearest integer, which is also coincidentally approximately 120π Ω. Some literature uses rounding to, for example, $\eta_0 \approx 376.73\ \Omega$.

Copyright © 2021 IEEE. All rights reserved.
Documents
Document Sharing Hub
Authorized licensed use limited to: Tsinghua University. Downloaded on March 06,2026 at 22:42:56 UTC from IEEE Xplore. Restrictions apply.
Full document details: IEEE 2889-2021

SAR	specific absorption rate
SB	skin block
TE	transverse electric (polarization)
TM	transverse magnetic (polarization)
VH	Visible Human
WG	working group

4. Physical and mathematical review of Poynting vector and power density

4.1 General

The assessment of the compliance of wireless devices in the millimeter wave frequency range is based on the assessment of the incident power density (IPD) in free space. The Poynting vector, on which the calculation of the IPD is based, consists of a single vector component in the far field only, whereas its characteristics are more complicated in the near field of an electromagnetic field source. Clause 4 gives an overview of the following:

— The Poynting theorem and the definition of the Poynting vector

— The definitions of the spatial-average power density (sPD) and the peak spatial-average power density (psPD)

4.2 Poynting theorem

The Poynting theorem is a statement of the conservation of energy for a configuration consisting of electric and magnetic fields acting on charges. The theorem is an energy balance indicating the rate of energy transfer (per unit volume) from a region of space is equal to the rate of work done on a charge distribution plus the energy flux leaving that region. This can be written as in Equation (1) (Durney, Massoudi, and Iskander [B5]):

$$\frac{\partial}{\partial t}\int_V \left(W_c + \frac{1}{2}\varepsilon E \cdot E + \frac{1}{2}\mu H \cdot H \right) dV + \oint_S \mathcal{E} x \mathcal{H} \cdot \boldsymbol{dS} = 0 \quad (1)$$

where

W_c	is the energy of the charged particles (including energy sources and losses, respectively) at a given point in the volume V
$(½)\varepsilon E \cdot E$	is the energy stored in the electric field (**E**-field) at a given point in V
$(½)\mu\, H \cdot H$	is the energy stored in the magnetic field **(H**-field) at a given point in V
$\mathcal{E}$	is the time-varying electric field vector to be distinguished from the complex phasor $\boldsymbol{E}$ introduced for the time-harmonic case in 4.3.2
$\mathcal{H}$	is the time-varying magnetic field vector to be distinguished from the complex phasor $\boldsymbol{H}$ introduced for the time-harmonic case in 4.3.2

A closed surface S is any surface that completely encloses the volume V. The integral over V corresponds to the total energy of all particles charged inside V and stored in the E-fields and H-fields. The first term at left is the time rate of change of the total energy inside V, which is total power. The second term on the left hand side is an integral over the closed mathematical surface enclosing V.

Copyright © 2021 IEEE. All rights reserved.
Documents
Document Sharing Hub
Authorized licensed use limited to: Tsinghua University. Downloaded on March 06,2026 at 22:42:56 UTC from IEEE Xplore. Restrictions apply.
Full document details: IEEE 2889-2021

4.3 Poynting vector and power density

4.3.1 General

In 4.3.2, $P(t)=\mathcal{E}(t)\times\mathcal{H}(t)$ is called the Poynting vector. It has units of watts per square meter and is interpreted as a power density. The direction of the cross product of E and H is perpendicular to both E and H.

The vector dot product of $\mathcal{E}\times\mathcal{H}$ and **dS** in Equation (1) selects the component of **P** that is parallel to d**S**. P(t) · d**S** is the power passing out through the differential surface element (**dS**), and the surface integral is the sum of the power passing through the **dS** elements over the entire surface (S), which is equal to the total power passing out through S (the total power flowing into the volume *V*).

The Poynting theorem can therefore be stated as follows: the time rate of change of the total energy inside *V* is equal to the negative of the total power passing outward through S.

4.3.2 Time average Poynting vector

The Poynting vector $P(t)=\mathcal{E}(t)\times\mathcal{H}(t)$ for time-harmonic variation can be written as in Equation (2):

$$\begin{aligned} P(t)&=\mathcal{E}\times\mathcal{H}=Re\left[\boldsymbol{E}\mathrm{e}^{\mathrm{j}\omega t}\right]\times Re\left[\boldsymbol{H}\mathrm{e}^{\mathrm{j}\omega t}\right]\\ &=\frac{1}{2}\left[\boldsymbol{E}\mathrm{e}^{\mathrm{j}\omega t}+\boldsymbol{E}^{*}\mathrm{e}^{-\mathrm{j}\omega t}\right]\times\frac{1}{2}\left[\boldsymbol{H}\mathrm{e}^{\mathrm{j}\omega t}+\boldsymbol{H}^{*}\mathrm{e}^{-\mathrm{j}\omega t}\right]\\ &=\frac{1}{2}Re\left[\boldsymbol{E}\times\boldsymbol{H}^{*}\right]+\frac{1}{2}Re\left[\boldsymbol{E}\times\boldsymbol{H}\mathrm{e}^{2\mathrm{j}\omega t}\right] \end{aligned} \tag{2}$$

where

E is a complex phasor field

H is a complex phasor field

* is the complex conjugate operator

The first term in Equation (2) is not a function of time, while the time variation of the second is twice the given frequency. Therefore, the time-averaged Poynting vector becomes as in Equation (3):

$$\boldsymbol{P}_{t\mathrm{Av}}=\frac{1}{2}Re\left[\boldsymbol{E}\times\boldsymbol{H}^{*}\right]\quad(\text{unit: W/m}^2) \tag{3}$$

The factor $\frac{1}{2}$ appears because $\dot{\boldsymbol{E}}$ and $\dot{\boldsymbol{H}}$ fields represent peak values.

4.3.3 Surface average Poynting vector

According to 4.3.2, the time average total power crossing the surface can be written as in Equation (4):

$$P_{\mathrm{tot}}=\oint_S\boldsymbol{P}_{\mathrm{tAv}}\cdot\boldsymbol{dS}=\frac{1}{2}\oint_S Re\left[\boldsymbol{E}\times\boldsymbol{H}^{*}\right]\cdot\boldsymbol{dS}\quad(\text{unit: W}) \tag{4}$$

Copyright © 2021 IEEE. All rights reserved.
Authorized licensed use limited to: Tsinghua University. Downloaded on March 06,2026 at 22:42:56 UTC from IEEE Xplore. Restrictions apply.
Full document details: IEEE 2889-2021

Performing a surface averaging of the above power from Equation (4), the spatial average of the power density (sPD) can be written as in Equation (5):

$$sPD_{\mathrm{n}} = \frac{1}{2A}\iint_A Re\left[\boldsymbol{E}\times\boldsymbol{H}^*\right]\cdot\boldsymbol{dA} \quad \text{(unit: W/m}^2\text{)} \tag{5}$$

where

A is the averaging area

$\boldsymbol{dA}$ is the differential area element vector

The quantity in Equation (5) is a power density. If A is a closed surface, using Equation (4) the power density of Equation (5) can be written as Equation (6):

$$sPD_{\mathrm{n}} = \frac{P_{\mathrm{tot}}}{A} \quad \text{(unit: W/m}^2\text{)} \tag{6}$$

Physically, the quantity of Equation (6) is therefore equivalent to a radiated power density uniformly distributed over the averaging area A and crossing this surface.

4.3.4 Discussion on surface averaged power density

To define a human exposure metric based on the Poynting theorem the following considerations need to be taken into account:

— The equations in 4.3.2 and 4.3.3 concern the incident power density in free space without any consideration of the interaction with a human body.

— In practice, the averaging area is not necessarily a closed surface.

— Practically, in the evaluation plane, the spatial averaging is done N times, where N is the number of points of the power density grid in the evaluation plane (see Figure 1).

— Generally, the power density is assessed in the near-field region of a radiating source, where the tangential components of the Poynting vector are not necessarily negligible compared to its surface-normal components.

Given the preceding items, another definition of surface averaged power density considering all three (or total) components of the Poynting vector is per Equation (7):

$$sPD_{\mathrm{tot}} = \frac{1}{2A}\iint_A \left\| Re\left[\boldsymbol{E}\times\boldsymbol{H}^*\right]\right\| \cdot dA \quad \text{(unit: W/m}^2\text{)} \tag{7}$$

In Equation (7), the double bars || … || represent the modulus (norm) of the vector.

Copyright © 2021 IEEE. All rights reserved.
Documents
Document Sharing Hub
Authorized licensed use limited to: Tsinghua University. Downloaded on March 06,2026 at 22:42:56 UTC from IEEE Xplore. Restrictions apply.
Full document details: IEEE 2889-2021

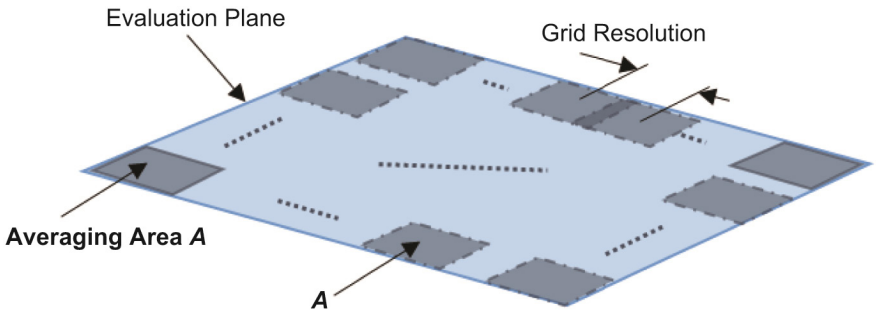


Figure 1 —Evaluation plane for the surface averaged power density

4.4 Comparison of the definitions of sPD

While Equation (7) does not have a clear physical meaning as does Equation (4), it is conservative with respect to Equation (5) and, when evaluated in free space without a body present, might better estimate the incident power density that will contribute to thermal elevation when a body is introduced. Therefore, the objective of this guide as mentioned in 1.1 is the assessment of both definitions to verify which of the two better correlates the sPD with the thermal elevation in human body tissues and therefore represents the more realistic approach.

5. Assessment methodology

5.1 General

This clause presents an overview of the methods that were used for the simulation of the electromagnetic fields in terms of the incident power density, for the quantification of the induced tissue heating, the experimental assessment of the incident power density and temperature increase, and the evaluation and presentation of the data. In detail, this includes the following:

— A brief description of the applied numerical electromagnetics solvers—which are the finite-difference time domain (FDTD) method, the finite integration technique (FIT), and the boundary element method (BEM)—which are used to calculate the IPD in free space and the transmitted power in the body phantoms

— An overview of the Pennes's bio-heat equation (PBHE), which is used to calculate the temperature increase in the body models as a function of the IPD

— A description of the measurement techniques and setups used for the experimental assessment of the IPD and the induced temperature increase for the validation of the numerical results

— The statistical methods which are used to determine the heating factors (HFs) and to demonstrate the statistical significance

5.2 Numerical methods

5.2.1 Electromagnetic simulations

Six organizations performed the simulations and provided/shared their results. The modeling group has performed the simulation of different sources at different frequencies, distances, and scenarios (see 6.1) in order to compare incident power density results using both definitions of Equation (5) and Equation (7), respectively.

Copyright © 2021 IEEE. All rights reserved.
Documents
Document Sharing Hub
Authorized licensed use limited to: Tsinghua University. Downloaded on March 06,2026 at 22:42:56 UTC from IEEE Xplore. Restrictions apply.
Full document details: IEEE 2889-2021

Several numerical techniques have been employed to evaluate the incident power density (IPD) in free-space and the SAR inside the simplified human block models. Specifically, FDTD has been adopted by four organizations, while the FIT and BEM have been employed by two other organizations. Depending on the adopted numerical technique, different boundary conditions (BCs) have been used to truncate the computational domain. Mainly, perfectly matched layers (PMLs) have been employed as absorbing BCs to reduce reflections of EM fields.

Two separate EM calculations were performed by each organization for each modeling scenario. First, the IPD in free-space was calculated without the presence of the body. Then, the simplified human block model was introduced (6.3), and field levels in tissue were calculated. In this latter case, the SAR, which is the input parameter for the temperature increase evaluation, has been calculated using the well-known expression of Equation (8):

$$SAR(\boldsymbol{r}) = \frac{\sigma(\boldsymbol{r})}{\rho(\boldsymbol{r})}\left|\boldsymbol{E}(\boldsymbol{r})\right|^2 \quad \text{(unit: W/kg)} \tag{8}$$

where

σ is the tissue conductivity (S/m)

ρ the mass density (kg/m^3)

$\boldsymbol{r}$ denotes the position vector in the coordinate system

5.2.2 Thermal simulations

Thermal calculations have been performed to obtain the time-varying tissue temperature (T) by solving the Pennes's bio-heat equation (PBHE) (Pennes [B20]), as expressed by Equation (9):

$$c(\boldsymbol{r})\rho(\boldsymbol{r})\frac{\partial T(\boldsymbol{r},t)}{\partial t} = \nabla\cdot\left[\kappa(\boldsymbol{r})\nabla T(\boldsymbol{r},t)\right] + \rho(\boldsymbol{r})SAR(\boldsymbol{r}) + \mathrm{A}(\boldsymbol{r},t) - \mathrm{B}(\boldsymbol{r},t)\left[T(\boldsymbol{r},t) - T_b(\boldsymbol{r},t)\right] \tag{9}$$

where

T is the temperature of the human tissue (°C)

T_b is the temperature of blood (°C)

κ is the thermal conductivity (W/(m K))

c is the heat capacity (J/(kg K))

A is the basal metabolism per unit volume (W/m^3)

B is a term associated with blood flow (W/(m^3 K))

At steady state, the temperature can be solved using Equation (10):

$$0 = \nabla\cdot\left[\kappa(\boldsymbol{r})\nabla T(\boldsymbol{r})\right] + \rho(\boldsymbol{r})SAR(\boldsymbol{r}) - \mathrm{B}(\boldsymbol{r})\left[T(\boldsymbol{r}) - T_b(\boldsymbol{r})\right] \tag{10}$$

The temperature elevation (ΔT) is the difference between temperatures obtained with and without EM exposure.

Copyright © 2021 IEEE. All rights reserved.
Documents
Document Sharing Hub
Authorized licensed use limited to: Tsinghua University. Downloaded on March 06,2026 at 22:42:56 UTC from IEEE Xplore. Restrictions apply.
Full document details: IEEE 2889-2021

Note that the coefficient representing the basal metabolism of the body does not impact the temperature increase due to electromagnetic field exposure when thermoregulatory responses are neglected, as considered in this guide. The BC for PBHE that describes the heat exchange between the air and the skin tissue is given by Equation (11):

$$-\kappa(\boldsymbol{r})\frac{\partial T(\boldsymbol{r},t)}{\partial n} = h\left[T_{\text{surf}}(\boldsymbol{r},t) - T_{\text{air}}(t)\right] \tag{11}$$

where

h is the heat transfer coefficient (W/(m^2 K))

T_{surf} is the surface temperature of the tissue (°C)

T_{air} is the air temperature (°C)

n is the normal vector at the boundary surface

Moreover, adiabatic BCs were set to all the inner boundaries, which are given by Equation (12):

$$\frac{\partial T(\boldsymbol{r},t)}{\partial n} = 0 \tag{12}$$

After the temperature increase is evaluated, the heating factors (HFs) can be defined as the ratio of the peak steady state temperature increase in the skin to the peak spatial-average power density per Equation (13):

$$\text{HF} = \frac{p\Delta T}{psPD} \tag{13}$$

5.3 Experimental methods

5.3.1 Measurements of the IPD

The measurement group members have performed the free space measurement of different sources at different frequencies, distances, and scenarios (see Table 1) in order to compare incident power density results using both definitions of Equation (5) and Equation (7), respectively. More details about the measurement scenarios are presented in 6.1. The results are presented in Clause 8 (summary of results) and Annex B with detailed distribution.

For each antenna type the following items are provided:

— Description of the device under test (Annex B)

— Measurement information (Annex B)

— Uncertainty budget (Annex B)

— Measurement results (described in Clause 8 and Annex B)

5.3.2 Thermographic measurements

The measurement setup is shown in Figure 2. An array antenna of 4 × 4 patches is used as radiation source at 60 GHz. The phantom was designed to obtain an equivalent temperature elevation to surface skin at

Copyright © 2021 IEEE. All rights reserved.
Documents
Document Sharing Hub
Authorized licensed use limited to: Tsinghua University. Downloaded on March 06,2026 at 22:42:56 UTC from IEEE Xplore. Restrictions apply.
Full document details: IEEE 2889-2021

steady state (Kawabata et al. [B16]). The ambient temperature was held at 24 °C, while the humidity was approximately 50% to 60%. Two exposure scenarios were considered, as schematically shown in Figure 3:

— Exposure scenario 1: the phantom aligned at boresight of the antenna

— Exposure scenario 2: the phantom tilted 30° from the boresight of the antenna

The separation distance between the antenna and the center of phantom surface was fixed to 70 mm. Note that the separation distance was determined to measure the surface temperature accurately with a thermographic camera. The surface temperature elevation was derived for an exposure duration of 30 min. Each measurement was repeated at least six times, and then mean and standard deviations were derived.

Power densities incident to the phantom were measured by over-the-air (OTA) measurement using a technique in Sasaki et al. [B22].

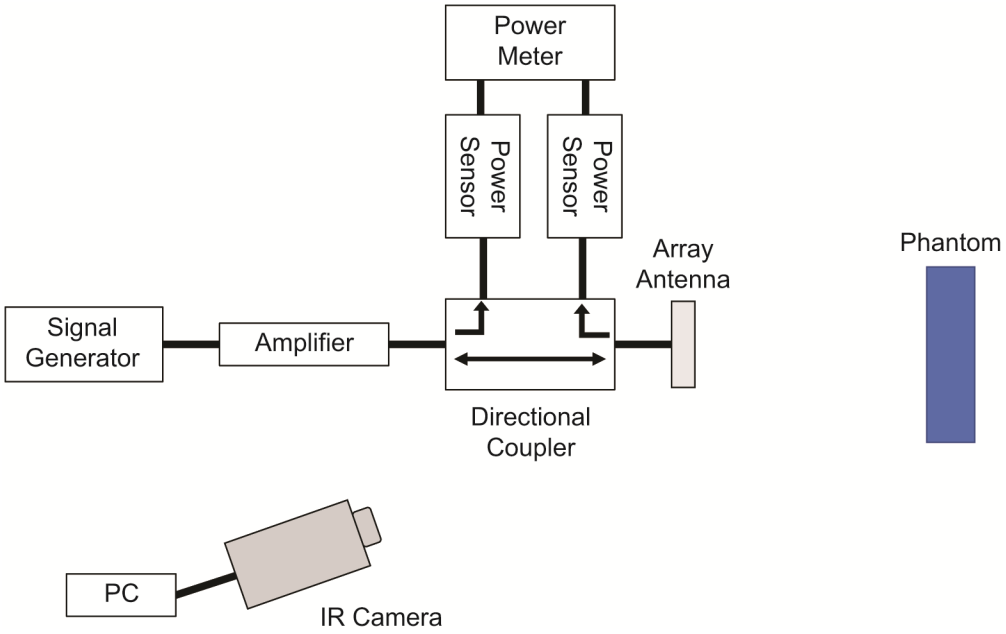


Figure 2—Schematic view of experimental setup for thermal measurements

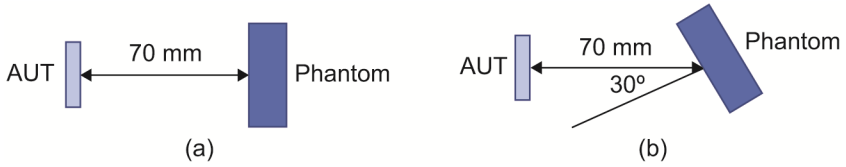


Figure 3—Exposure scenario (a) #1 and (b) #2

Copyright © 2021 IEEE. All rights reserved.
Authorized licensed use limited to: Tsinghua University. Downloaded on March 06,2026 at 22:42:56 UTC from IEEE Xplore. Restrictions apply.
Full document details: IEEE 2889-2021

5.4 Evaluation and analysis of the results

5.4.1 General

In the context of this guide, the statistical approach applied allows the calculation of a correlation coefficient between the IPD and the temperature rise when these are considered as random variables. Multiple exposure configurations simulated by different organizations are used to perform the statistical analysis of this correlation.

The evaluation of the results provided by the modeling ad-hoc group started with the data collection and aggregation in specific tables. Note that the provided data comprised all the computed peak values of IPD arranged by:

— The spatial-average values sPD_n and sPD_{tot}

— Averaging areas of 1 cm^2 and 4 cm^2

— Temperature increase ΔT for the different simulation scenarios

The data collected include:

— Institution/research group

— EM source

— Frequency of the EM signal

— Distance between the source and the body phantom

Since all the groups have provided the data for the dipole (unlike more sparse data available for other EM sources), the analyses have been performed on two macro-groups or data sets:

— Dipole source, all simulated distances and frequencies, consisting of 115 samples

— All sources (including dipole), all simulated scenarios, consisting of 227 samples

In the following, the first macro-group will be named *dipole data*, and the second macro-group will be named *all data*.

5.4.2 sPD versus Δ*T* scatter plots

The first analysis has been conducted to analyze the scatter plots of the peak spatial-average power densities, *psPD,* data, and the respective values of peak temperature increase, $p\Delta T$. Specifically, the following pairs of data series have been plotted, first for *dipole data*, then for the *all data*:

— ($psPD_n$ avg.1, $p\Delta T$)

— ($psPD_{tot}$ avg.1, $p\Delta T$)

— ($psPD_n$ avg.4, $p\Delta T$)

— ($psPD_{tot}$ avg.4, $p\Delta T$)

where

avg.1 corresponds to the results obtained by using an averaging area of 1 cm^2

avg.4 corresponds to the results obtained by using an averaging area of 4 cm^2

Copyright © 2021 IEEE. All rights reserved.
Documents
Document Sharing Hub
Authorized licensed use limited to: Tsinghua University. Downloaded on March 06,2026 at 22:42:56 UTC from IEEE Xplore. Restrictions apply.
Full document details: IEEE 2889-2021

A distinction has been highlighted between the data coming from the simulations with distance $d = 2$ mm and the data from all other simulation scenarios with $d \geq 5$ mm, to evaluate possible influence of near-field exposure condition. The scatter plots were aimed at visually establishing the type of correlation (linear or not) and its strength (i.e., strong, weak, or no correlation).

5.4.3 Heating factor analysis

After generating the scatter plots for all data series, the HFs (5.2.2) have been analyzed, grouping the results by institution/research group. To this end, the average value (μ_{HF}) and standard deviation (σ_{HF}) for each group have been computed for each of the four metrics—namely HF_{n} avg.1, HF_{tot} avg.1, HF_{n} avg.4, and HF_{tot} avg.4—and for the combined arrays of (HF_{n} avg.1, HF_{n} avg.4) as well as (HF_{tot} avg.1, HF_{tot} avg.4). The same computations have been also repeated considering the data from all groups together. The standard deviation of each HF sample was of particular interest, since a smaller value of σ_{HF} would suggest stronger correlation with ΔT. Finally, for each PD metric, the relative frequencies of the HF occurrences (computed for all the data set) have been plotted to examine their distribution around the average value μ_{HF}.

5.4.4 Pearson's correlation coefficients

The Pearson's correlation coefficients have been computed to identify the PD metric that best correlates with the temperature increase ΔT. The coefficients describe the linear correlation between the *psPD* data sets (different metrics) and $p\Delta T$. Specifically:

- r_{n1} is the Pearson's coefficient of the pair ($psPD_{\mathrm{n}}$ avg.1, $p\Delta T$)
- r_{tot1} is the Pearson's coefficient of the pair ($psPD_{\mathrm{tot}}$ avg.1, $p\Delta T$)
- r_{n4} is the Pearson's coefficient of the pair ($psPD_{\mathrm{n}}$ avg.4, $p\Delta T$)
- r_{tot4} is the Pearson's coefficient of the pair ($psPD_{\mathrm{tot}}$ avg.4, $p\Delta T$)

Equation (14) was employed for the computation of the coefficient (Walpole, et al. [B25]):

$$r_{lk} = \frac{\mathrm{Cov}\left(psPD_l\ avg.k, p\Delta T\right)}{\sigma\left(psPD_l\ avg.k\right)\sigma\left(p\Delta T\right)}, \quad l = \mathrm{n, tot} \quad k = 1, 4 \tag{14}$$

where

$\mathrm{Cov}(psPD_{\mathrm{l}}$ avg.k, $p\Delta T)$ is the covariance of $psPD_{\mathrm{l}}$ avg.k and $p\Delta T$

$\sigma(psPD_{\mathrm{l}}$ avg.k) is the the standard deviation of $psPD_{\mathrm{l}}$ avg.k

$\sigma(p\Delta T)$ is the standard deviation of $p\Delta T$

Notice that each set of four different r_{lk} have been computed distinguishing results for 2 mm distance between antenna and phantom and results for all other data distances:

- r_{n1}, r_{tot1}, r_{n4}, r_{tot4} for *dipole data* corresponding to $d \geq 5$ mm
- r_{n1}, r_{tot1}, r_{n4}, r_{tot4} for all *dipole data* (thus, including data corresponding to $d = 2$ mm)
- r_{n1}, r_{tot1}, r_{n4}, r_{tot4} for *all data* corresponding to $d \geq 5$ mm
- r_{n1}, r_{tot1}, r_{n4}, r_{tot4} for the whole *all data* set (thus, including data corresponding to $d = 2$ mm)

Copyright © 2021 IEEE. All rights reserved.
Documents
Document Sharing Hub
Authorized licensed use limited to: Tsinghua University. Downloaded on March 06,2026 at 22:42:56 UTC from IEEE Xplore. Restrictions apply.
Full document details: IEEE 2889-2021

5.4.5 Statistical significance test

To consolidate the conclusions, a statistical significance test on the correlation coefficients has been performed. Such a procedure is also helpful to check whether the noise in the analyzed data had significantly affected the computed values of r_{lk}. In particular, it could be analyzed if the probability that the difference between r_{im} and r_{jn}, $i \neq j$ or $m \neq n$, is merely due to chance (i.e., noise in the data) is less than a significance level α (e.g., $\alpha = 5\%$ if a confidence level of 95% is chosen). A simplified scheme of the statistical hypothesis testing procedure hereby adopted is described as follows:

a) The first step is to state the relevant *null* and *alternative hypotheses*. In our case, the null hypothesis is H_0: $\rho_{im} = \rho_{jn}$, $i \neq j$ or $m \neq n$, where ρ_{im} and ρ_{jn} are the **true** correlation coefficients (of which r_{im} and r_{jn} are estimators) of the pairs of data samples (sPD_i avg.m, ΔT) and (sPD_j avg.n, ΔT). The alternative hypothesis is H_1: $\rho_{im} > \rho_{jn}$, i, j, m, n such that $\rho_{im} > \rho_{jn}$.

b) Choose the appropriate test and state the relevant test statistic. Since the compared correlations are overlapping, i.e., they have one variable in common (the temperature increase ΔT), the set of test statistics for dependent correlations provided by the *cocor* package have been used (Diedenhofen, and Musch [B4]).

c) Establish a significance level α. In this case, a value of $\alpha = 5\%$ has been adopted.

d) Compute the values of the test statistic from the observed data. This means computing the *z*-scores or *t*-scores associated to the difference between correlation coefficients: $r_{im} - r_{jn}$.

e) Decide to either reject the null hypothesis in favor of the alternative or not reject it. The decision rule is to reject the null hypothesis H_0 if the observed value $r_{im} - r_{jn}$ is in the critical region, and to accept or "fail to reject" the hypothesis otherwise.

The last two steps of the process are automatically performed by the tool provided in the *cocor* package.

6. Exposure configurations

6.1 General

6.1.1 Study design

As outlined in 1.1, this study is an investigation of the induced temperature increase in the skin for exposure to the near field and the far field of antennas considering a large distance and frequency range from 2 mm to 150 mm and 10 GHz to 90 GHz, respectively, as well as different antenna dimensions with respect to the wavelength. The antenna models are summarized in 6.2. The distance range in terms of wavelength is given in Table 1.

In most configurations, the antennas expose the anatomical models in boresight. For some antenna array cases the effect of beam shift (oblique incidence) was studied.

Because the penetration depth in human tissue in this frequency range does not exceed 5 mm in the frequency range of this study, only the body surface is considered by the body models. Different stratified skin models and one anatomical model of the ear region are taken into account. These models are summarized in 6.3. The applied dielectric and thermal parameters are given in 6.4.

Subclause 5.4 discusses the evaluation of the results with the objective to establish a definition of the IPD that best correlates with the heating factor considering the different components of the Poynting vector and sizes of the averaging areas, and it introduces the statistical methods that are applied in the final analysis of the results.

Copyright © 2021 IEEE. All rights reserved.
Documents
Document Sharing Hub
Authorized licensed use limited to: Tsinghua University. Downloaded on March 06,2026 at 22:42:56 UTC from IEEE Xplore. Restrictions apply.
Full document details: IEEE 2889-2021

Both the electromagnetic and the thermal evaluations are carried out numerically using different techniques. These are summarized in 5.2.1 and 5.2.2. A subset of the results is validated experimentally as described in Annex B.

In addition to the configurations of Table 1, the impact of the incident angle is evaluated numerically and experimentally. The configurations are discussed in 6.5, and their evaluation is presented separately in 7.7 and 10.3.

Table 1—Distances in terms of wavelength

Frequency	Distance				
	2 mm	5 mm	10 mm	50 mm	150 mm
10 GHz	$\lambda/15$	$\lambda/6$	$\lambda/3$	$5\lambda/3$	5λ
30 GHz	$\lambda/5$	$\lambda/2$	1λ	5λ	15λ
60 GHz	$2\lambda/5$	1λ	2λ	10λ	30λ
90 GHz	$3\lambda/5$	$3\lambda/2$	3λ	15λ	45λ

6.1.2 Implementation

The study was carried out in a joint effort of six different laboratories. The antenna models for the numerical simulations are described in 6.2. The numerical models of the skin are developed or provided by the participating laboratories. It should be noted that not all configurations of antennas, distances, and skin models were evaluated by all participating laboratories. Moreover, minor deviations of the applied thermal tissue parameters and boundary conditions occurred, which were considered in the statistical analysis (7.3). Table 2 gives an overview of the configurations evaluated numerically by the participating laboratories.

Experimental results of the IPD (free space) were provided by one laboratory. The configurations are given in Table 3. Thermographic validation measurements were conducted by another lab for the patch array antenna of 6.2.5.

For each antenna type the following elements are provided in the detailed description of the results in Annex B:

- Description of the device under test
- Measurement information
- Uncertainty budget
- Measurement results (Clause 8 and Annex B)

Copyright © 2021 IEEE. All rights reserved.
Authorized licensed use limited to: Tsinghua University. Downloaded on March 06,2026 at 22:42:56 UTC from IEEE Xplore. Restrictions apply.
Full document details: IEEE 2889-2021

Table 2—Configurations simulated by the different laboratories: Details of the body models, their dielectric and thermal parameters, and the antenna models are given in 6.2, 6.3, and 6.4

Lab	Body model	Thermal parameter set	Half-wavelength dipole	Dipole antenna array	Cavity fed array	Patch antenna	Patch array	Pyramidal horn
#1	L1	1	f GHz: 10, 30, 60 spacing, mm: 2, 5, 10	f GHz: 10, 30, 60 spacing, mm: 2, 5, 10, 50, 150	—	f GHz: 30 spacing, mm: 2, 5, 10	f GHz: 30 spacing, mm: 2, 5, 10	—
#2	L2	2	f GHz: 10, 30, 60, 90 spacing, mm: 2, 5, 10, 50, 150	—	—	—	—	—
#3	L3	3	f GHz: 10, 30, 60, 90 spacing, mm: 2, 5, 10, 50, 150	f GHz: 10, 30, 60, 90 spacing, mm: 2, 5, 10, 50, 150	—	—	—	—
#4	H2, A	4	f GHz: 10, 30, 60 spacing, mm: 2, 5, 10, 50, 150	—	—	—	—	f GHz: 30, 60 spacing, mm: 2, 5, 10, 50
#5	H1	5	f GHz: 10, 30, 60, 90 spacing, mm: 2, 5, 10, 50, 150	—	f GHz: 10, 90 spacing, mm: 2	—	—	f GHz: 10, 90 spacing, mm: 2
#6	L3	6	f GHz: 10, 30, 60, 90 spacing, mm: 2, 5, 10, 50	—	—	—	—	—

Table 3—Measurement scenarios

Antenna type	Frequencies (GHz)	Exposure evaluation distance (mm)
Cavity-fed dipole array	10, 30, 60, 90	2, 5, 10, 50, 150
Pyramidal horn slotted array	10, 30, 60, 90	2, 5, 10, 50, 150
WiGig mockup	58.32, 60.48, 62.64	2, 5, 10, 50

6.2 Numerical antenna models

6.2.1 Half-wavelength dipole

A standard half-wavelength dipole, modeled as perfect electric conductor (PEC), and designed for the frequencies of 10 GHz, 30 GHz, 60 GHz, and 90 GHz has been used. The distance d between the antenna and the body model was 2 mm, 5 mm, 10 mm, 50 mm, and 150 mm. The antenna accepted power was normalized to 10 mW.

Copyright © 2021 IEEE. All rights reserved.
Documents
Document Sharing Hub
Authorized licensed use limited to: Tsinghua University. Downloaded on March 06,2026 at 22:42:56 UTC from IEEE Xplore. Restrictions apply.
Full document details: IEEE 2889-2021

6.2.2 Dipole antenna array

A 4 × 4-element dipole antenna array for the frequencies of 10 GHz, 30 GHz, 60 GHz, and 90 GHz has been used (see Figure 4). Each dipole element was separated to each other by $\lambda/2$. The distance d between the antenna and the body model was 2 mm, 5 mm, 10 mm, 50 mm, and 150 mm. The antenna results are normalized to a total accepted power of 10 mW equally distributed over all antenna elements.

Three different cases were considered for the phase shift between the elements of the antenna:

— Beam in boresight, i.e., no phase shift between elements

— Beam shift in azimuth, i.e., the phases of the 16 elements were:

0°, 135°, 270°, 45°

0°, 135°, 270°, 45°

0°, 135°, 270°, 45°

0°, 135°, 270°, 45°

— Beam shift in elevation, i.e., the phases of the 16 elements were:

0°, 0°, 0°, 0°

135°, 135°, 135°, 135°

270°, 270°, 270°, 270°

45°, 45°, 45°, 45°

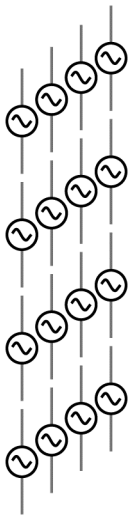


Figure 4 —Dipole array antenna

Copyright © 2021 IEEE. All rights reserved.
Authorized licensed use limited to: Tsinghua University. Downloaded on March 06,2026 at 22:42:56 UTC from IEEE Xplore. Restrictions apply.
Full document details: IEEE 2889-2021

6.2.3 Cavity-fed array

The specific computer-aided design (CAD)–based model of this antenna has been employed in this study (see Figure 5). The cavity is fed with a wave-guide source in TE10 mode. The E-field of the TE10 mode points into the y direction of the coordinate system of the model. The location and the extension of the source are indicated in the CAD file, while the solid absorber ($\varepsilon_r = 1$, $\sigma = 0.5$ S/m) attenuates the fields in the waveguide for faster decay of the energy in the cavity. The substrate has the following dielectric properties: $\varepsilon_r = 3.62$, $\sigma = 0.0326$ S/m. The antenna is scaled for operation at 10 GHz, 30 GHz, 60 GHz, and 90 GHz. The antenna accepted power was normalized to 10 mW.

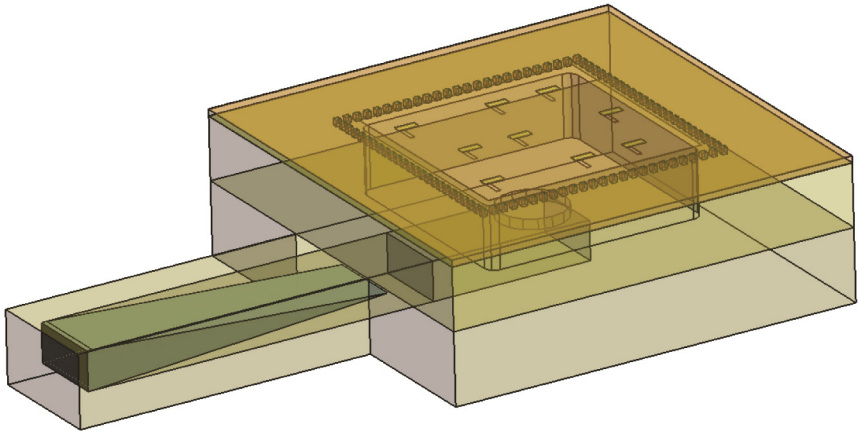


Figure 5 —Cavity-fed dipole array

6.2.4 Patch antenna

A square patch antenna at the frequency of 30 GHz has been used. The dimensions are shown in Figure 6. The patch has a 100 mm × 100 mm dielectric substrate with ε_r of 2.2 (Teflon) and thickness of 0.6 mm. The length of the patch element is 0.3λ (3 mm at 30 GHz). The distance d between the antenna and the body model was 2 mm, 5 mm, and 10 mm. The antenna accepted power was normalized to 10 mW.

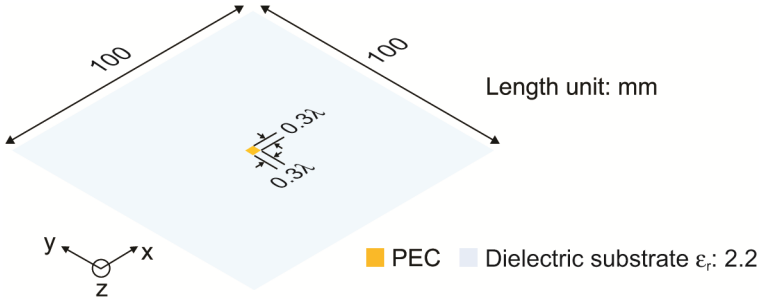


Figure 6 —Dimension of patch antenna at 30 GHz

6.2.5 Patch array

A standard 4 × 4 patch array antenna based on the single patch element described in 6.3.1 has been used. The dimensions are shown in Figure 7. The patch has a 100 mm × 100 mm dielectric substrate with ε_r of

Copyright © 2021 IEEE. All rights reserved.
Documents
Document Sharing Hub
Authorized licensed use limited to: Tsinghua University. Downloaded on March 06,2026 at 22:42:56 UTC from IEEE Xplore. Restrictions apply.
Full document details: IEEE 2889-2021

2.2 (Teflon) and thickness of 0.6 mm. The length of the patch element is 0.3λ (3 mm at 30 GHz), while the separation distance between each element is 0.5λ (5 mm at 30 GHz). The operating frequency was 30 GHz, while the distance *d* between the antenna and the body model was 2 mm, 5 mm, and 10 mm. The antenna output power was normalized to 10 mW with equally distributed over all antenna elements. All three cases of phase shift were considered i.e., boresight, shift in azimuth, shift in elevation.

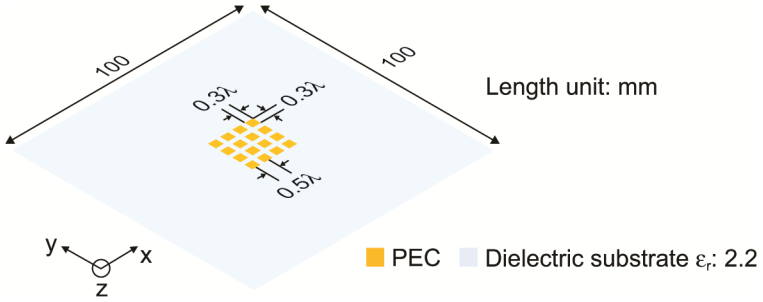


Figure 7—Dimension of 4 × 4 patch array antenna at 30 GHz used by organization #1

6.2.6 Pyramidal horn slotted array

The CAD file of the pyramidal horn with slot array was provided in SAT format (see Figure 8). The horn is fed with a lumped source which connects the solid PEC_monopole to ground. A source resistance of 50 Ω is suggested. The antenna is scaled for operation at 30 GHz and 60 GHz. All the five distances *d* between the antenna and the body model were considered. The antenna accepted power was normalized to 10 mW.

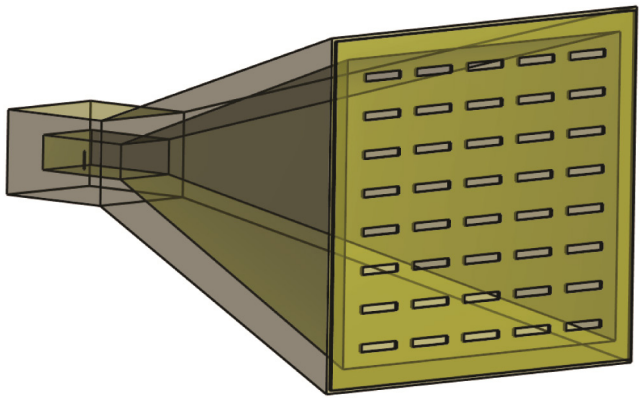


Figure 8 —Pyramidal horn with slot array

6.3 Numerical body models

6.3.1 Homogenous body model H1

Body model H1 is a single-layer simplified skin block model as shown in Figure 9. The numerical solver was the FDTD with a uniform grid resolution having a step size Δ as reported in Table 4. For dipole array and slot array working at 10 GHz, a smaller body model dimensions (a × b × c, where a = 75 mm, b = 150 mm, c = 150 mm) was used. For dipole array and slot array working at 90 GHz, a grid resolution of 0.125 mm was used instead of that specified in Table 4. The computational domain was truncated with a low reflection PML-BC. Tissue dielectric properties are reported in 6.4.1.

Copyright © 2021 IEEE. All rights reserved.
Documents
Document Sharing Hub
Authorized licensed use limited to: Tsinghua University. Downloaded on March 06,2026 at 22:42:56 UTC from IEEE Xplore. Restrictions apply.
Full document details: IEEE 2889-2021

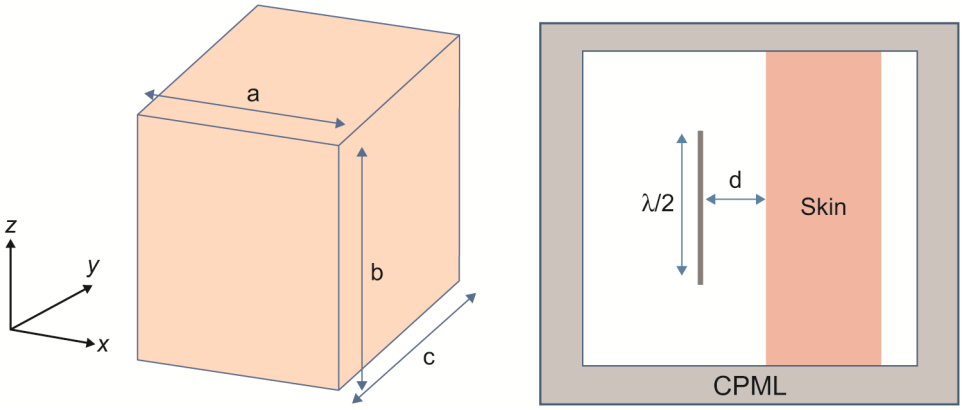


Figure 9 —Body models and computational domain

Table 4—Model dimensions and grid resolution

Dimensions	Frequency (GHz)			
	10	**30**	**60**	**90**
a (mm)	100	75	50	30
b (mm)	200	150	100	60
c (mm)	200	150	100	60
Δ (mm)	0.5	0.25	0.125	0.0625

6.3.2 Multi-layer body model L1

A simplified four-layer model with the dimensions reported in Figure 10 has been employed (Kawabata et al. [B16]). The model is composed of the epidermis (0.2 mm), dermis (1.0 mm), subcutaneous fat (3.8 mm), and muscle (15 mm). Tissue dielectric properties presented in Figure 12 have been assigned. The EM problem was solved using an in-house FDTD solver with a uniform grid resolution Δ of 0.2 mm for the frequencies of 10 GHz and 30 GHz and 0.1 mm at 60 GHz (see details in Table 5). The computational domain was truncated by ten-layer Berenger's perfectly matched layer BCs.

Copyright © 2021 IEEE. All rights reserved.
Documents
Document Sharing Hub
Authorized licensed use limited to: Tsinghua University. Downloaded on March 06,2026 at 22:42:56 UTC from IEEE Xplore. Restrictions apply.
Full document details: IEEE 2889-2021

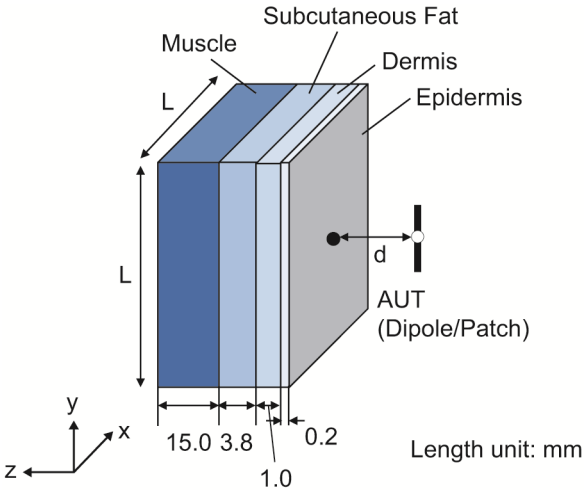


Figure 10—Body model L1

Table 5—Model dimensions and grid resolution of L1

Dimensions	Frequency (GHz)		
	10	30	60
L (mm)	100	100	50
Δ (mm)	0.2	0.2	0.1

6.3.3 Multi-layer body model L2

A simplified three-layer model with the dimensions reported in Figure 11 has been employed. The width (L_y) and height (L_z) of the body model were equal to each other (L) and chosen as listed in Table 6. Tissue dielectric properties have been assigned by (Gabriel, Lau, and Gabriel [B8]). The numerical solver was an ad-hoc FDTD code with a uniform grid resolution Δ as reported in Table 6. The computational domain was truncated with a ten-layer convolutional perfectly matched layer boundary condition (CPML-BC).

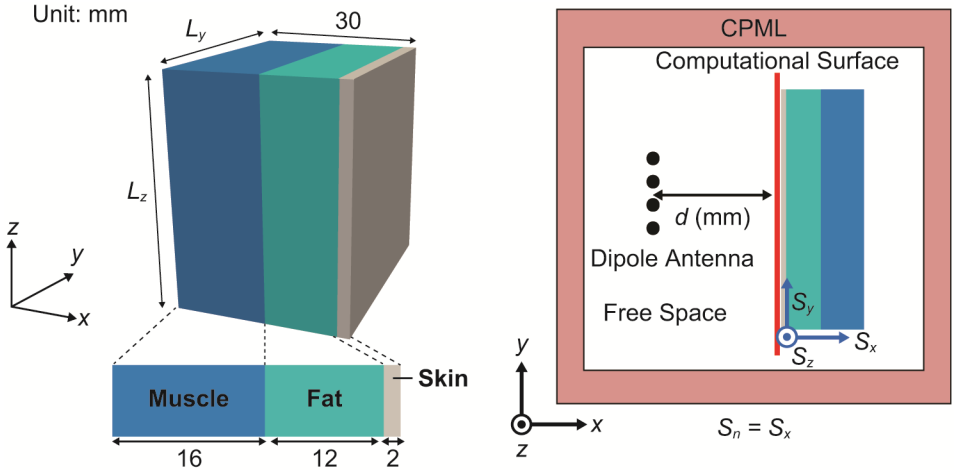


Figure 11—Body model and computational domain of L2

Copyright © 2021 IEEE. All rights reserved.
Documents
Document Sharing Hub
Authorized licensed use limited to: Tsinghua University. Downloaded on March 06,2026 at 22:42:56 UTC from IEEE Xplore. Restrictions apply.
Full document details: IEEE 2889-2021

Table 6—Model dimensions and grid resolution of L2

Dimensions	Frequency (GHz)			
	10	30	60	90
L (mm)	400	200	100	80
Δ (mm)	0.5	0.25	0.125	0.1

6.3.4 Multi-layer body model L3

A simplified three-layer model with the dimensions reported in Figure 12 has been employed. The numerical solver was an in-house FDTD code with a uniform grid resolution Δ as reported in Table 7. The computational domain was truncated with a ten-layer CPML-BC. Tissue dielectric properties are reported in Table 9.

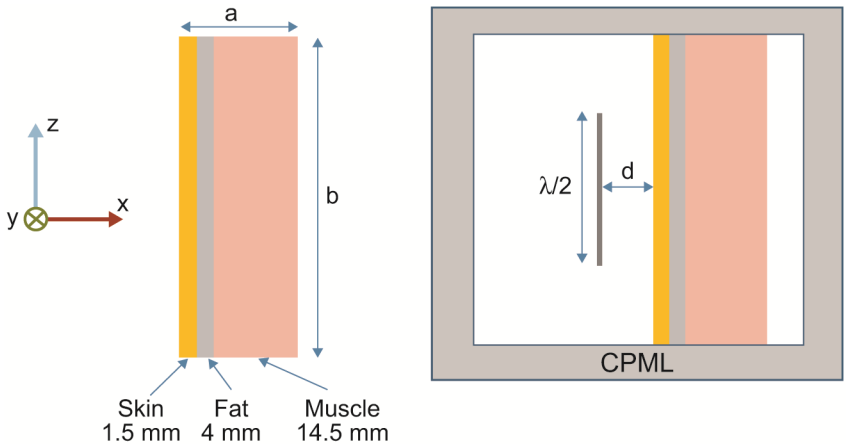


Figure 12—Body model and computational domain of L3

Table 7—Model dimensions and grid resolution of L3

Dimensions	Frequency (GHz)			
	10	30	60	90
a (mm)	20	20	20	20
b (mm)	100	50	50	50
Δ (mm)	0.5	0.25	0.125	0.1

6.3.5 Homogenous body model H2

Body model H2 is a single-layer simplified skin block model as shown in Figure 9. The numerical solver was the FIT with a non-uniform grid resolution having a maximum step size Δ_{max} and a minimum step size Δ_{min} as reported in Table 8. The computational domain was truncated with a CPML-BC with an estimated reflection of 10^{-4}. Tissue dielectric properties are reported in 6.4.1.

Copyright © 2021 IEEE. All rights reserved.
Documents
Document Sharing Hub
Authorized licensed use limited to: Tsinghua University. Downloaded on March 06,2026 at 22:42:56 UTC from IEEE Xplore. Restrictions apply.
Full document details: IEEE 2889-2021

Table 8—Model dimensions and grid resolution of H2

Dimensions	Frequency (GHz)		
	10	**30**	**60**
a (mm)	100	50	40
b (mm)	200	150	80
c (mm)	200	150	80
Δ_{max} (mm)	1.63	0.75	0.3
Δ_{min} (mm)	0.15	0.1	0.05

6.3.6 Anatomical body model A

A realistic heterogeneous model of the Visible Human (VH) (Figure 13), has been employed. The numerical solver was the FIT with a non-uniform grid resolution having a maximum step size Δ_{max} and a minimum step size Δ_{min} as reported in Table 9. The computational domain was truncated with a CPML-BC with an estimated reflection of 10^{-4}. Tissue dielectric properties are reported in 6.4.1.

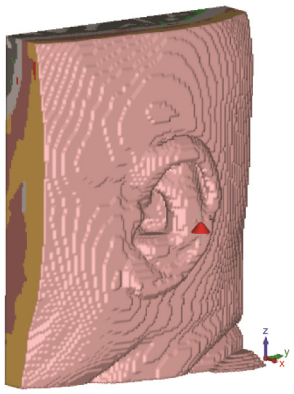


Figure 13—Visible Human (HUGO) model

Table 9—Model dimensions and grid resolution used for the anatomical body model A

Dimensions	Frequency (GHz)		
	10	**30**	**60**
a (mm)	40	31	31
b (mm)	117	86	86
c (mm)	154	93	93
Δ_{max} (mm)	1.65	0.55	0.3
Δ_{min} (mm)	0.15	0.1	0.05

Copyright © 2021 IEEE. All rights reserved.
Documents
Document Sharing Hub
Authorized licensed use limited to: Tsinghua University. Downloaded on March 06,2026 at 22:42:56 UTC from IEEE Xplore. Restrictions apply.
Full document details: IEEE 2889-2021

6.4 Tissue parameters

6.4.1 Dielectric parameters

The dielectric tissue parameters for the layered generic body models L1, L2, and L3, for the homogeneous body model H2 and for the anatomical body model A are taken from the five-term Cole-Cole model described in (Gabriel, Lau, and Gabriel [B8]). They are summarized in Table 10. The parameters of the homogeneous body model H1 are given in Table 11.

Table 10—Dielectric tissue properties used for the multilayer body models and for the anatomical body model

(a) Multilayer body model L1 (6.3.2)

Tissue	10 GHz		30 GHz		60 GHz	
	σ (S/m)	ϵ_r	σ (S/m)	ϵ_r	σ (S/m)	ϵ_r
Epidermis	5.40	25.99	21.32	15.66	33.14	8.52
Dermis	7.88	32.75	26.80	18.48	39.57	10.43
Fat	3.14	14.60	10.85	8.53	15.50	5.73
Muscle	10.03	37.92	32.21	19.56	46.32	10.67

(b) Multilayer body models L2 (6.3.3), L3 (6.3.4), and anatomical body model A (6.3.6)

Tissue	10 GHz		30 GHz		60 GHz		90 GHz	
	σ (S/m)	ϵ_r	σ (S/m)	ϵ_r	σ (S/m)	ϵ_r	σ (S/m)	ϵ_r
Skin	8.4824	32.409	27.31	16.63	37.96	9.096	41.94	6.826
Fat	0.585	4.602	1.794	3.639	2.815	3.132	3.411	2.931
Muscle	10.63	42.76	35.49	23.16	52.83	12.86	60.72	9.304
Air inside body	0.00	1.00	0.00	1.00	0.00	1.00	—	—
Blood	13.13	45.11	38.80	22.56	54.72	12.28	—	—
Bone cortical	2.14	8.12	5.15	5.01	7.21	3.81	—	—
Bone spongiosa	3.86	12.66	9.26	7.23	13.17	5.06	—	—
Brain grey matter	10.31	38.11	31.76	19.88	45.62	11.19	—	—
Brain white matter	7.30	28.40	22.61	15.37	32.53	9.17	—	—
Cartilage	9.02	25.63	20.74	12.58	27.48	8.05	—	—
Cerebrospinal fluid	15.38	52.43	46.00	26.59	65.76	14.18	—	—
Salivary glands	12.13	45.15	38.12	23.19	54.89	12.66	—	—

Copyright © 2021 IEEE. All rights reserved.
Documents
Document Sharing Hub
Authorized licensed use limited to: Tsinghua University. Downloaded on March 06,2026 at 22:42:56 UTC from IEEE Xplore. Restrictions apply.
Full document details: IEEE 2889-2021

Table 11—Dielectric tissue properties used for the body model H1 (6.3.1)

Tissue	10 GHz		30 GHz		60 GHz		90 GHz	
	σ (S/m)	ϵ_r	σ (S/m)	ϵ_r	σ (S/m)	ϵ_r	σ (S/m)	ϵ_r
Skin	8.014	31.29	27.10	15.51	36.40	7.97	38.99	5.94

6.4.2 Thermal parameters

6.4.2.1 General

The thermal parameters were not specified explicitly but left to the participating laboratories to choose. They are described in 6.4.2.2 through 6.4.2.7.

6.4.2.2 Thermal parameter set 1

The heat transfer coefficient between the skin and air was set to $h = 10$ W/(m^2 °C). The air and (arterial) blood temperature in the core of T_{air} and T_b were set to 20 °C and 37 °C, respectively. Tissue thermal properties were taken from Kawabata et al. [B16] and are summarized in Table 12.

Table 12—Set 1 of thermal properties used for the layered body model

Parameter	Epidermis	Dermis	Subcutaneous fat	Muscle
k (W/(m K))	0.42	0.42	0.25	0.50
ρ (kg/m^3)	1109	1109	911	1090
B (W/(m^3 K))	0	9100	1700	2700

6.4.2.3 Thermal parameter set 2

Tissue thermal properties were taken by Hirata et al. [B12], except for the skin blood perfusion (Foster, Ziskin, and Balzano [B6]), and are reported in Table 13. The heat transfer coefficient between the skin and air was set to $h = 8$ W/(m^2 K). The air and body core temperature of T_{air} and T_b were set to 20 °C and 37 °C, respectively. All the other BCs were set to adiabatic. The same T_{air} and T_b were used for sets 3 through 6 of thermal parameter.

Table 13—Set 2 of thermal properties used for the layered body model

Parameter	Epidermis	Dermis	Muscle
k (W/(m K))	0.42	0.25	0.50
ρ (kg/m^3)	1125	916	1047
B (W/(m^3 K))	7505	1626	2700

6.4.2.4 Thermal parameter set 3

The heat convection at the air-skin interface was employed using a convection coefficient $h = 8$ W/(m^2·K), while for the other boundaries adiabatic conditions were employed. Tissue thermal properties are taken by Hasgall et al. [B9] and are reported in Table 14.

Copyright © 2021 IEEE. All rights reserved.
Documents
Document Sharing Hub
Authorized licensed use limited to: Tsinghua University. Downloaded on March 06,2026 at 22:42:56 UTC from IEEE Xplore. Restrictions apply.
Full document details: IEEE 2889-2021

Table 14—Set 3 of thermal properties used for the layered body model

Parameter	Epidermis	Dermis	Muscle
k (W/(m K))	0.37	0.21	0.49
ρ (kg/m^3)	1109	911	1090
B (W/(m^3 K))	7441	1903	2691

6.4.2.5 Thermal parameter set 4 for body models H2 and A

The air-skin interface was modeled by a convective BC with a heat transfer coefficient $h = 8$ W/(m^2 K). Adiabatic BCs were employed for all other surfaces. Tissue thermal properties are reported in Table 15.

Table 15—Set 4 of thermal properties used for body models H2 and A

Tissue	Density (kg/m^3)	Thermal conductivity (W/(m K))	Blood flow (W/(m^3 K))
Air inside body	0	0.02	0
Blood	1050	0.50	1E+06
Bone cortical	2000	0.40	3E+03
Bone spongiosa	1200	0.40	3E+03
Brain grey matter	1050	0.50	4E+04
Brain white matter	1040	0.50	2E+04
Cartilage	1100	0.60	9E+03
Cerebrospinal fluid	1010	0.60	0
Fat	900	0.20	2E+03
Muscle	1080	0.50	3E+03
Salivary glands	1040	0.60	4E+05
Skin	1100	0.30	9E+03

6.4.2.6 Thermal parameter set 5

The air-skin interface was modeled by a convective BC with a heat transfer coefficient $h = 8$ W/(m^2 K). Adiabatic BCs were employed for all other surfaces. Tissue thermal properties are reported in Table 16.

Table 16—Set 5 of thermal properties used for the layered body model

Tissue	Density (kg/m^3)	Thermal conductivity (W/(m K))	Specific heat (J/(kg K))	Blood flow (W/(m^3 K))
Skin	1100	0.37	3400	2230

6.4.2.7 Thermal parameter set 6

Thermal calculations have been performed solving the PBHE with a FEM approach. The heat convection at the air-skin interface was employed using a convection coefficient h = 10 W/(m^2·K), while for the other boundaries adiabatic conditions were employed. Tissue thermal properties are reported in Table 17.

Copyright © 2021 IEEE. All rights reserved.
Documents
Document Sharing Hub
Authorized licensed use limited to: Tsinghua University. Downloaded on March 06,2026 at 22:42:56 UTC from IEEE Xplore. Restrictions apply.
Full document details: IEEE 2889-2021

Table 17—Set 6 of thermal properties used for the layered body model

Parameter	Epidermis	Dermis	Muscle
k (W/(m K))	0.42	0.25	0.50
ρ (kg/m^3)	1109	911	1090
B (W/(m^3 K))	9100	1700	2700

6.5 Influence of incidence angles

The effects of incidence angle of a plane wave impinging on a block human model when using both definitions of Equation (5) and Equation (7), respectively, has been analyzed. The description of the exposure scenarios is showed in Table 18.

Table 18—Summary of exposure scenarios

Organization	Polarization	Source type	Incident angles (°)	Frequencies (GHz)	Evaluation distance (mm)
Lab #1	Transverse electric (TE), transverse magnetic (TM)	Plane wave	0 to 90	30	—
Lab #3	TE, TM	4 × 4 dipole array	0, 15, 30, 45	30, 60	30
Lab #2	TE, TM	4 × 1 dipole array, 8 × 1 dipole array	0, 15, 30, 45, 60 (TE and TM) 75, 80 (TM)	28	15 (TE, 4 × 1 array), 30 (TM, 4 × 1 array), 45 (TE and TM, 8 × 1 array)

Note that the minimum distance (15 mm) is larger than the one applied for the configurations outlined in 6.1 because a certain distance is needed to form a beam when considering an oblique incidence. In addition, the block model is inclined to realize an incident angle of 75° and 80°. As mentioned in Nakae et al. [B19], the angle of incidence is difficult to define in the near field, and thus the angle from the array center to the place where the maximum Poynting vector was observed at the surface of the model was used.

7. Numerical results

7.1 General

Clause 7 summarizes the numerical results for the heating factor provided by the participating laboratories for all combinations of antennas and body models and discusses the applicability of the different PD metrics with respect to their correlation to the temperature increase. In detail, the analysis is carried out in the following steps:

- Discussion of the temperature increase as a function of the IPD for the pooled results of the different laboratories
- Analysis of the dependence of the heating factor on the distance between antenna and phantom
- Statistical evaluation of the results in terms of mean value and standard deviation as well as evaluation of the Pearson's correlation coefficients
- Discussion of the statistical significance

The complete results provided by each laboratory are given in Annex A.

Copyright © 2021 IEEE. All rights reserved.
Documents
Document Sharing Hub
Authorized licensed use limited to: Tsinghua University. Downloaded on March 06,2026 at 22:42:56 UTC from IEEE Xplore. Restrictions apply.
Full document details: IEEE 2889-2021

7.2 Pooled temperature increase versus incident power density

For the derivation of the heating factor, the paired numerical results of the IPD and the temperature increase are evaluated in terms of scatter plots for the different PD metrics (normal and total) and averaging areas (1 cm^2 and 4 cm^2). The scatter plots are shown in Figure 14 through Figure 17, and Figure 18 through Figure 21, for the dipole only and all antennas, respectively. In these plots, regression lines given by the equation $y_i = s_i\, x$, with $i = 5$, 2 referring to data with $d \geq 5$ mm or $d \geq 2$ mm, have been included. A quantification of possible effects of these data on the correlation coefficients is given in 7.4.

The results rearranged as plots of the heating factors as a function of electric distance, distinguished by the PD definition (HF_n versus HF_{tot}), are reported in Figure 22 and Figure 23 for the 1 cm^2 and 4 cm^2 avg. metrics, respectively. The graphical evaluation of the plots shows that the average value of HF_n is constantly greater than the one of HF_{tot}, but their difference diminishes with electrical distance because the tangential components of the Poynting vector tend to zero in the far field. Moreover, the greater dispersion around the average value (higher standard deviation) of HF_n is also evident.

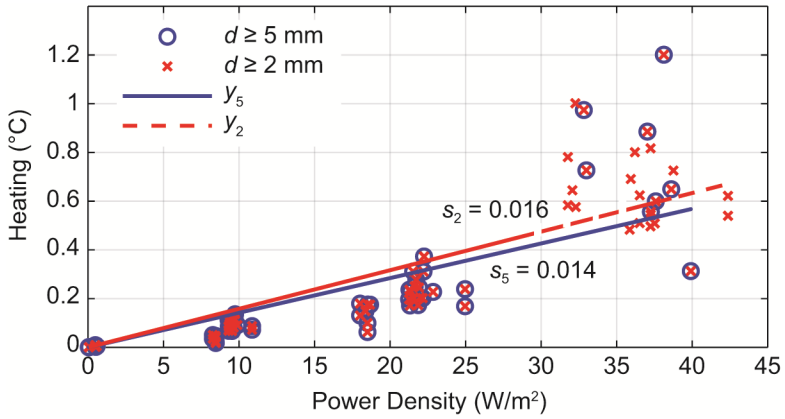


Figure 14—*psPD*$_n$ avg.1 versus *pΔT* dipole data scatter plot

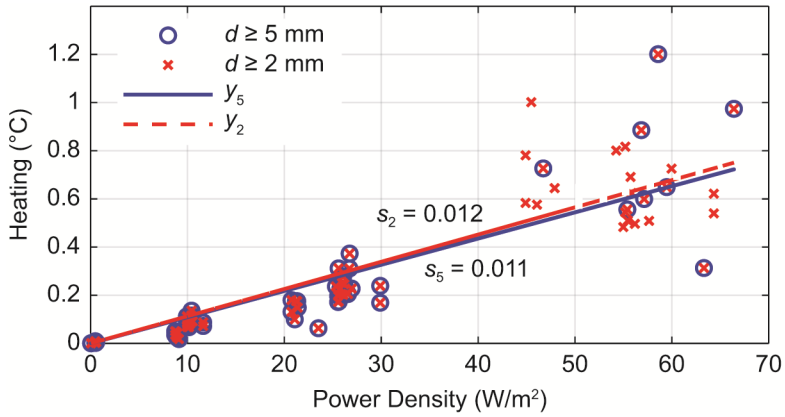


Figure 15—*psPD*$_{tot}$ avg.1 versus *pΔT* dipole data scatter plot

Copyright © 2021 IEEE. All rights reserved.
Authorized licensed use limited to: Tsinghua University. Downloaded on March 06,2026 at 22:42:56 UTC from IEEE Xplore. Restrictions apply.
Full document details: IEEE 2889-2021

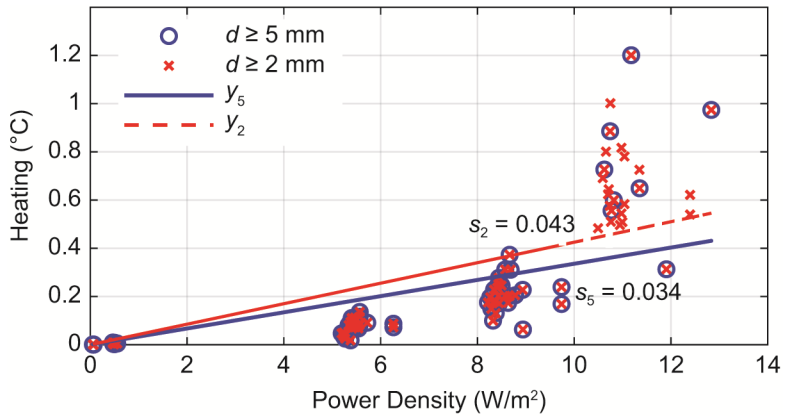


Figure 16 —*psPD*$_n$ avg.4 versus *pΔT* dipole data scatter plot

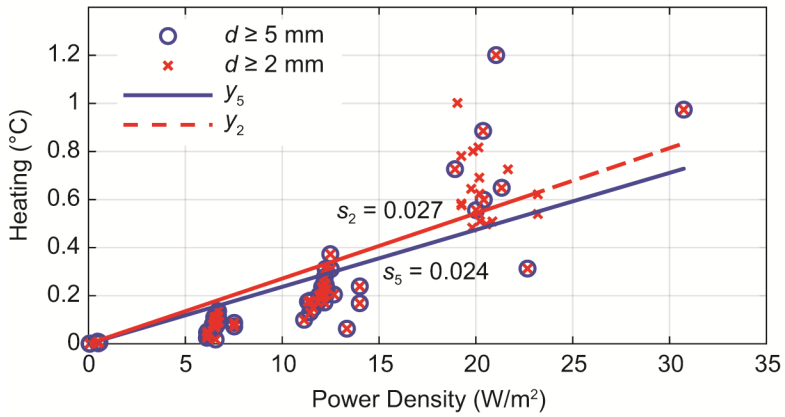


Figure 17 —*psPD*$_{tot}$ avg.4 versus *pΔT* dipole data scatter plot

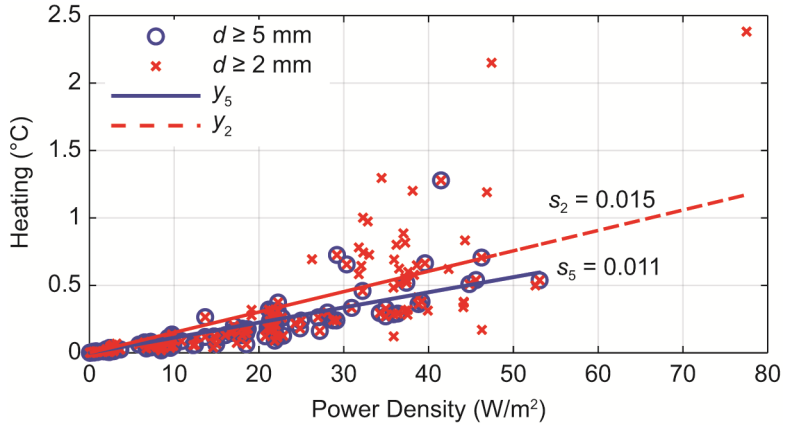


Figure 18 —*psPD*$_n$ avg.1 versus *pΔT* all data scatter plot

Copyright © 2021 IEEE. All rights reserved.
Documents
Document Sharing Hub
Authorized licensed use limited to: Tsinghua University. Downloaded on March 06,2026 at 22:42:56 UTC from IEEE Xplore. Restrictions apply.
Full document details: IEEE 2889-2021

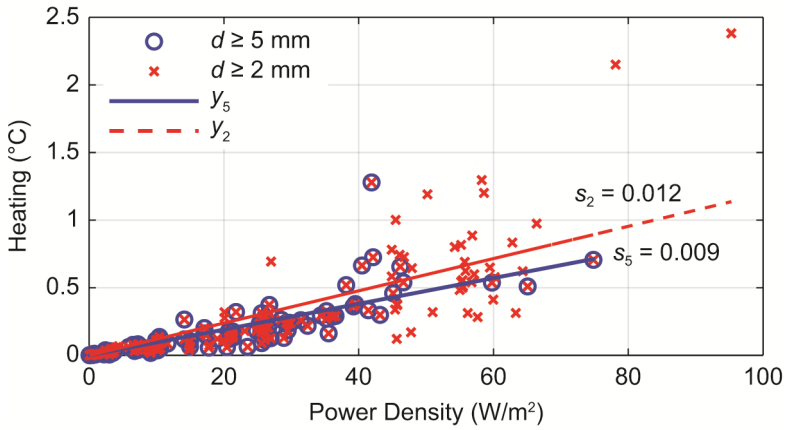


Figure 19 —*psPD*$_{tot}$ avg.1 versus *pΔT* all data scatter plot

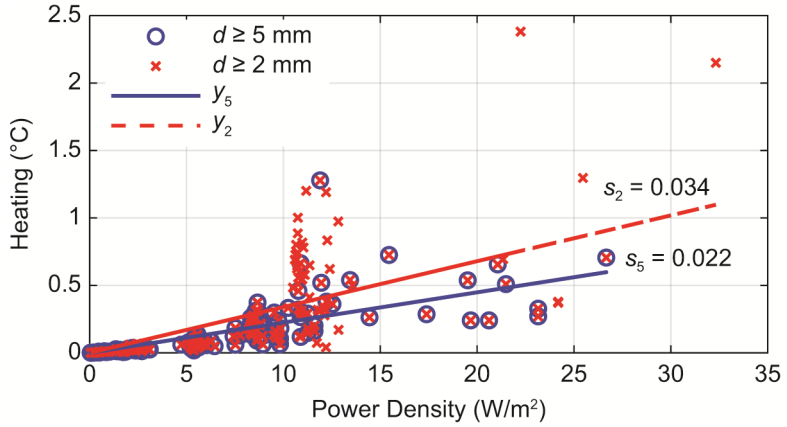


Figure 20 —*psPD*$_{n}$ avg.4 versus *pΔT* all data scatter plot

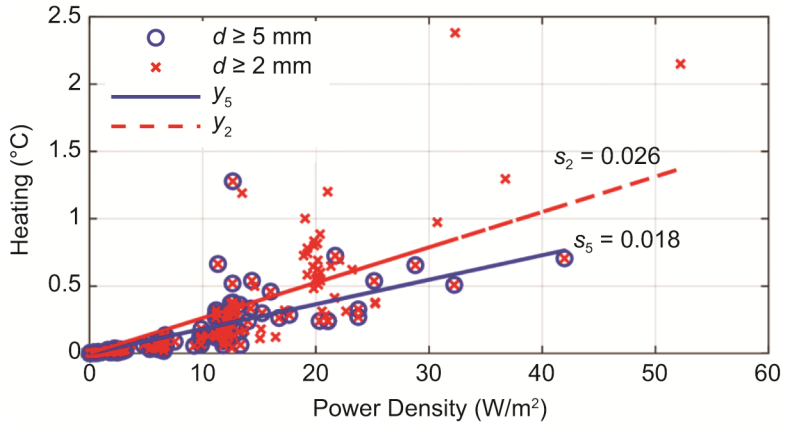
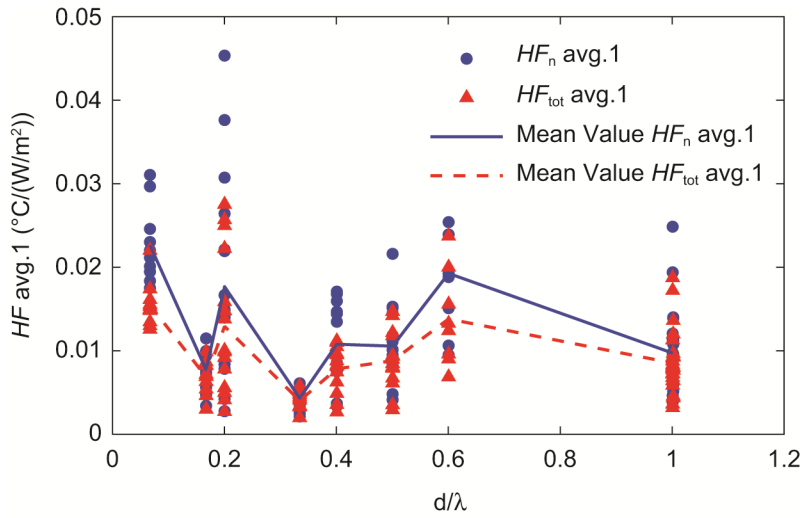
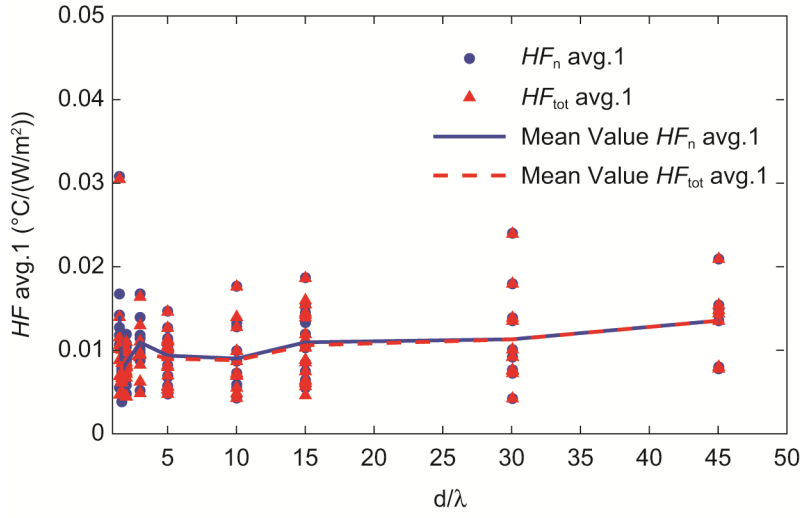


Figure 21 —*psPD*$_{tot}$ avg.4 versus *pΔT* all data scatter plot

Copyright © 2021 IEEE. All rights reserved.
Authorized licensed use limited to: Tsinghua University. Downloaded on March 06,2026 at 22:42:56 UTC from IEEE Xplore. Restrictions apply.
Full document details: IEEE 2889-2021



(a)



(b)

Figure 22—HF_n avg.1 (blue) and HF_{tot} avg.1 (red) plotted against electric distance from 0 to 1 (a) and 1 to 45 (b)

Copyright © 2021 IEEE. All rights reserved.
Documents
Document Sharing Hub
Authorized licensed use limited to: Tsinghua University. Downloaded on March 06,2026 at 22:42:56 UTC from IEEE Xplore. Restrictions apply.
Full document details: IEEE 2889-2021

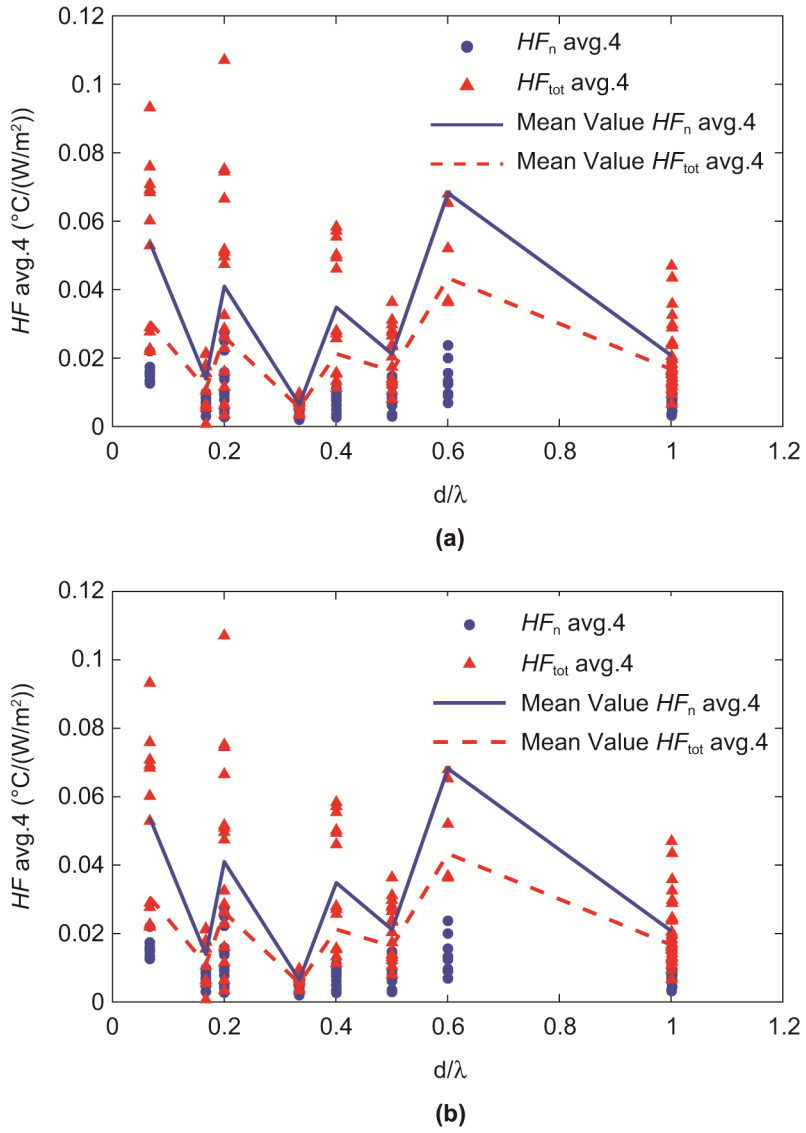


Figure 23 —HF_n avg.4 (blue) and HF_{tot} avg.4 (red) plotted against electric distance from 0 to 1 (a) and 1 to 45 (b)

7.3 Heating factors—statistical analysis

Table 19 shows the relative standard deviations of the HFs for the different PD metrics (normal and total) and averaging areas (1 cm^2 and 4 cm^2).

The results in Table 19 show that the metric $psPD_{tot}$ yields the lowest relative standard deviation, except for the Lab #2 values, where both metrics are nevertheless comparable. The bold values indicate the HF distributions with the smallest relative standard deviation.

The frequency distributions of the heating factors are shown in Figure 24 through Figure 27. The average value of each distribution is outlined with a dotted vertical red line.

Moreover, the HF data has been transformed, computing their logarithm to obtain closer to normal distributions. This allows a more significant analysis of the corresponding relative standard deviations. The frequency distributions of the logarithms of HF are shown in Figure 28 through Figure 31. The associated

Copyright © 2021 IEEE. All rights reserved.
Documents
Document Sharing Hub
Authorized licensed use limited to: Tsinghua University. Downloaded on March 06,2026 at 22:42:56 UTC from IEEE Xplore. Restrictions apply.
Full document details: IEEE 2889-2021

relative standard deviations are reported in Table 20. As in the case of HF, relative standard deviations coming from the logarithms of HF_{tot} definitions have smaller values than those coming from the logarithms of HF_n.

Table 19—HF relative standard deviations (%) sorted by PD metric and research group

Research group	σ (HF_n avg. 1)	σ (HF_{tot} avg. 1)	σ (HF_n avg. 4)	σ (HF_{tot} avg. 4)
Lab #1	61.67	**51.82**	71.00	60.68
Lab #2	**46.72**	49.26	90.05	92.88
Lab #3	44.06	**43.94**	84.97	83.67
Lab #4	44.53	**40.08**	81.96	53.75
Lab #5	35.19	**34.34**	73.88	46.35
Lab #6	62.44	**47.68**	96.14	69.84
All	57.02	**49.58**	90.09	76.95

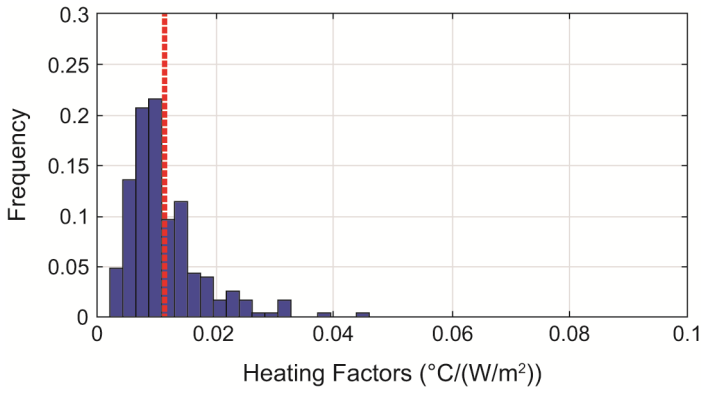


Figure 24—Occurrences distribution of HF_n avg.1; red dotted line is the average value

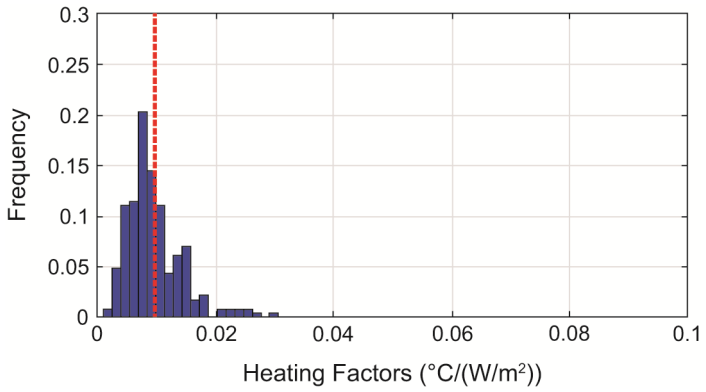


Figure 25—Frequencies distribution of HF_{tot} avg.1; red dotted line is the average value

Copyright © 2021 IEEE. All rights reserved.
Documents
Document Sharing Hub
Authorized licensed use limited to: Tsinghua University. Downloaded on March 06,2026 at 22:42:56 UTC from IEEE Xplore. Restrictions apply.
Full document details: IEEE 2889-2021